increased the myoglobin levels compared with the baseline level, suggesting that acute myocardial ischemia disrupted the plasma membrane of the myocardium, allowing myoglobin to leak into the myocardial interstitium. The myoglobin level during the last 15 min of ischemia reached, on average, 12 times the baseline myoglobin level. Reperfusion further increased the myoglobin level. The myoglobin level during the first 15 min of reperfusion was, on average, three times higher than the myoglobin level during the last 15 min of ischemia. After 15 min of reperfusion, the myoglobin level declined gradually with time but remained higher than the baseline level until the last 15 min of the reperfusion period. In the VS group, the time course was similar but the changes in the myoglobin levels during the ischemia and reperfusion periods were smaller than those observed in the VX group. In the VS-W group, changes in the myoglobin levels were attenuated compared to those observed in the VX group and no significant increase in myoglobin was detected upon reperfusion. In the VS-P group, changes in the myoglobin levels showed intermediate values, which were between those observed in the VX and VS groups.

Baseline myoglobin levels were not significantly different among the VX, VS, VS-W, and VS-P groups (157±40, 110±23, 124±48, and 118±30 ng/ml, respectively). Average myoglobin levels for the ischemic period (Fig. 2A), reperfusion period (Fig. 2B), and total period (Fig. 2C) were significantly lower in the VS and VS-W groups compared with the VX group.

Changes in HR are summarized in the top panel of Fig. 3. Baseline HR did not markedly differ among the four groups. In the VS group (filled circles), vagal stimulation decreased the HR throughout the ischemic and reperfusion periods compared with the HR in the VX group (open circles). After the cessation of vagal stimulation (denoted as "vagal stim off"), the HR in the VS group returned toward the baseline level. In the VS-W group (double circles), vagal stimulation decreased the HR at 15 and 30 min compared with the results from the VX group. Although the HR from 45 to 120 min did not differ significantly compared with the VX group, the cessation of vagal stimulation increased the HR, suggesting that vagal stimulation was effective until the end of the reperfusion period. In the VS-P group (open squares), the HR was maintained at 200 beats/min using ventricular pacing. The cessation of ventricular pacing (denoted as "pacing off") significantly decreased the HR below the baseline level, suggesting that vagal stimulation was effective during the ventricular pacing.

Changes in AP are summarized in the bottom panel of Fig. 3. Differences in AP between the VS and VX groups were not statistically significant. Although pretreatment with wortmannin increased the AP in the VS-W group, differences in AP between the VS-W and VX groups were not statistically significant at any time point. In the VS-P group, AP at 15 min was significantly lower compared with that in the VX group.

Discussion

Vagal stimulation-induced cardioprotection against ischemic injury

Cardiac microdialysis is a useful method to monitor changes in myocardial interstitial myoglobin levels in an ischemic region (Kitagawa et al., 2005). LAD occlusion increased the myoglobin level in the myocardial interstitium in the VX group (Fig. 1). Vagal stimulation, initiated immediately after the LAD occlusion, suppressed myoglobin release during ischemia (Figs. 1 and 2A). In addition to preventing lethal ventricular arrhythmia during acute myocardial ischemia (Myers et al., 1974; Rosenshtraukh et al., 1994; Vanoli et al., 1991), vagal stimulation also appears to reduce myocardial damage in the ischemic region. Because we avoided large ischemia by occluding LAD just distal to the first diagonal branch, lethal ventricular

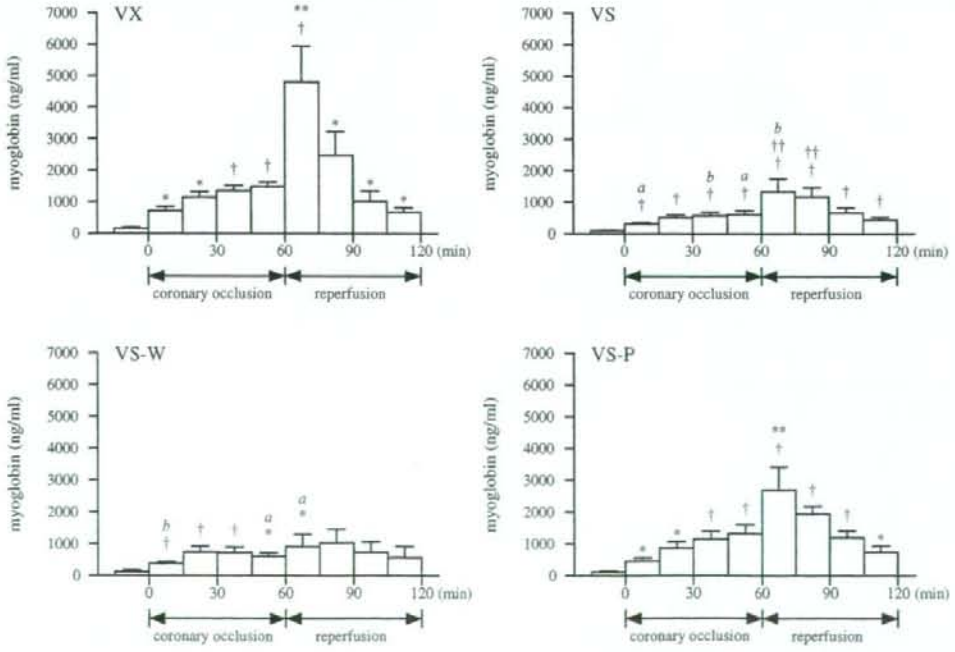

Fig. 1. Changes in the myocardial interstitial myoglobin levels in the VX, VS, VS-W, and VS-P groups. After collecting baseline dialysate samples, the left anterior descending coronary artery was occluded for 60 min and then reperfused for 60 min. Acute myocardial ischemia significantly increased the myoglobin level in the ischemic region. Reperfusion further increased the myoglobin level. Data are shown as the means+SE ($n=6$ each). †$P<0.01$ and *$P<0.05$ compared with the baseline value. ††$P<0.01$ and **$P<0.05$ compared with the myoglobin level during the last 15 min of ischemia. $^{a}P<0.01$ and $^{b}P<0.05$ compared with the corresponding myoglobin level in the VX group.

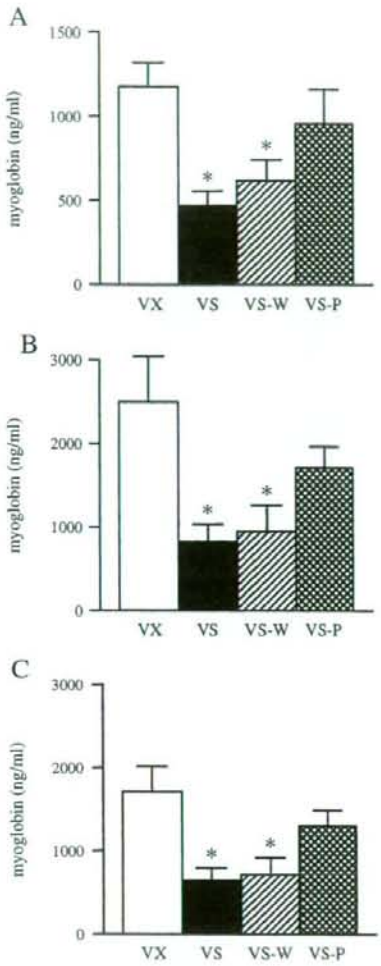

Fig. 2. Average myoglobin levels for the ischemic period (A), reperfusion period (B), and total period throughout ischemia and reperfusion (C). In all panels, the myoglobin levels were significantly lower in the vagal stimulation (VS) and vagal stimulation with wortmannin pretreatment (VS-W) groups than in the control, vagotomized (VX) group. The myoglobin levels in the vagal stimulation with fixed-rate pacing (VS-P) group did not markedly differ from those in the VX group. Data are shown as the means + SE ($n = 6$ each). *$P < 0.05$ compared with the VX group.

arrhythmia scarcely occurred in the present experimental settings. The cardioprotective effect induced by vagal stimulation may include direct effects of ACh on the ischemic myocardium and indirect effects induced through altered hemodynamics.

For the direct effects, ACh administered prior to a coronary artery occlusion can exert a preconditioning mimetic effect via a signaling pathway that includes PI3K (Qin et al., 2003; Oldenburg et al., 2003). Because we initiated vagal stimulation immediately after the LAD occlusion, however, the mechanism underlying the reduced myocardial damage observed in the present study is likely independent of the preconditioning mimetic effect. In support of this interpretation, the inhibition of PI3K did not affect the reduced myoglobin release induced by vagal stimulation (Fig. 2A, VS-W group). The results of the present study, however, did not preclude the direct involvement of ACh through mechanisms other than the PI3K pathway.

For the indirect effects, bradycardia reduces myocardial oxygen consumption by decreasing the number of ventricular contractions per unit time (Sammel et al., 1983; Shinke et al., 1999). Vagal stimulation also dilates normal coronary arteries via ACh and vasoactive intestinal polypeptide release (Feigl, 1969; Reid et al., 1985; Feliciano and Henning, 1998; Henning and Sawmiller, 2001), which may increase collateral flow into the ischemic region. Bradycardia associated with vagal stimulation may increase coronary perfusion due to a prolonged diastolic interval (Buck et al., 1981), reduced ventricular contractility via a force-frequency mechanism (Maughan et al., 1985), and antagonism of the sympathetic effect (Nakayama et al., 2001). These processes may have improved the balance between energy supply and demand, leading to reduced myocardial injury in the ischemic region. In the present study, the VS-P group showed myoglobin levels that were between those of the VX and VS groups (Fig. 2A), suggesting that bradycardia plays a significant role in vagally induced cardioprotection. The observed effect of fixed-rate ventricular pacing on the vagal effect agrees with our previous study (Kawada et al., 2006), in which prevention of bradycardia using ventricular pacing abolished the suppressive effect of vagal stimulation on the ischemia-induced increase in myocardial interstitial norepinephrine levels.

Reperfusion-induced myocardial injury

Reperfusion of the LAD increased the myocardial interstitial myoglobin level compared with that detected during the last 15 min of ischemia (Fig. 1), which agreed with in vivo observations in the rabbit heart (Kitagawa et al., 2005). In the isolated perfused rat heart, 30 min of hypoxia or anoxia increased the concentration of creatinine kinase in the interstitial transudate, an effect that was further augmented by reoxygenation (Wienen and Kammermeier, 1988). The increased levels of these macromolecules upon reperfusion may have resulted from a reperfusion injury. During ischemia, ATP deficiency impairs the operation of Na^+/K^+ ATPases, resulting in the accumulation of intracellular Na^+. Ischemia also causes acidosis in the ischemic region. Upon reperfusion, washing out the excess extracellular H^+ promotes intracellular Na^+ accumulation via Na^+/H^+ exchange. Eventually, Ca^{2+} influx occurs due to reverse-mode operation of Na^+/Ca^{2+} exchangers (Lazdunski et al., 1985). Once the intracellular Ca^{2+} concentration reaches a threshold level, ATP resynthesis causes hypercontracture of myofibrils and cytoskeletal lesions (Piper, 1989; Piper et al., 2004). Additionally, the recovery of myocardial contraction upon reperfusion increases the leakage of

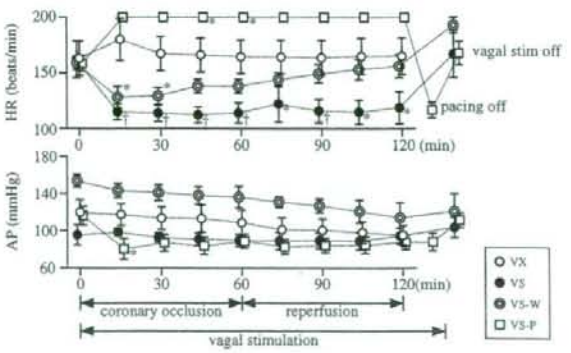

Fig. 3. Changes in heart rate (HR) and arterial pressure (AP). The HR and AP data immediately before the coronary occlusion are shown at time 0. In the vagal stimulation (VX) and vagal stimulation with wortmannin pretreatment (VS-W) groups, cessation of vagal stimulation increased the HR, suggesting that vagal stimulation was effective until the end of the reperfusion period. In the vagal stimulation with fixed-rate pacing group (VS-P), cessation of pacing decreased the HR, whereas cessation of vagal stimulation increased the HR, suggesting that vagal stimulation was effective during ventricular pacing. Data are shown as the means ± SE ($n = 6$ each). †$P < 0.01$ and *$P < 0.05$ compared with the corresponding data from the VX group.

cytosolic molecules from damaged sarcolemmal membranes. For example, ventricular wall stress increases the leakage of lactate dehydrogenase after anoxia in K^+-arrested, isolated, perfused rat heart (Takami et al., 1990). These two explanations are not mutually exclusive and both may contribute to the increased myocardial interstitial myoglobin levels during reperfusion.

In the present study, vagal stimulation significantly reduced the myoglobin levels in the VS and VS-W groups during the reperfusion period (Fig. 2B). The reduced myoglobin levels during the reperfusion period correlated with the decreased myoglobin levels during the ischemic period. It is likely that reduced myocardial injury during the ischemic period contributed to the inhibition of myocardial injury during the reperfusion period. Further studies that include stimulating the vagal nerve during the ischemic or reperfusion period separately may be required to identify the respective effects of vagal stimulation during each of these potentially deleterious events. Although the PI3K signaling pathway played a significant role in the prevention of reperfusion injury by low-pressure reperfusion and postconditioning in the isolated rat heart (Bopassa et al., 2006), the inhibition of PI3K by wortmannin did not antagonize the reduction in myoglobin release induced by vagal stimulation in the present study. The fact that wortmannin inhibits superoxide release from polymorphonuclear leukocytes and exerts cardioprotective effects during myocardial ischemia and reperfusion (Young et al., 2000) makes it difficult to interpret the in vivo effects of wortmannin in blood perfused hearts.

Reperfusion is a pre-requisite to salvaging viable myocardium, following an acute myocardial infarction (Hausenloy and Yellon, 2004). Possible clinical relevance of vagal stimulation is that vagal stimulation may be able to reduce myocardial damage associated with the reperfusion therapy. Endovascular approach (Nabutovsky et al., 2007) may be feasible for vagal stimulation in acute clinical settings. In a long-term treatment, we have shown that intermittent vagal stimulation improves the survival of chronic heart failure following myocardial infarction in rats (Li et al., 2004). On the other hand, bradycardic therapy using a sinus node inhibitor cilobradine also improves left ventricular function and remodeling of chronic heart failure in dogs (Cheng et al., 2007). Although whether bradycardic therapy is equivalent to vagal stimulation remains a matter of investigation, vagal stimulation may be an additional strategy for treatment of myocardial infarction and chronic heart failure.

Limitations

There are several limitations to the present study. First, we did not quantify the infarct size. Although the measurement of myocardial interstitial myoglobin levels are useful to monitor the time course of myocardial injury development, further studies are required to determine the correlation between the local myoglobin levels and infarct size. Second, HR in the VX group declined to approximately 165 beats/min with time elapsed, resulting in the higher HR in the VS-P group than in the VX group. Although the fixed-rate pacing partially reversed the vagally induced protective effect, slowing the pacing rate might have lowered the myoglobin levels in the VS-P group similar to VS group. Finally, while the inhibition of PI3K signaling pathway by pretreatment of wortmannin did not abolish the vagally induced protective effect, expression and/or activation of PI3K signaling pathway components in the ischemic target tissues was not examined. Further studies focusing on the molecular and cellular basis are required to identify the mechanism(s) by which vagal stimulation attenuates the myocardial injury.

Conclusion

Vagal nerve stimulation, initiated immediately after LAD occlusion, reduced myocardial injury as assessed by myocardial interstitial myoglobin levels. The direct effects of ACh on the ischemic myocardium, at least those associated with the PI3K signaling pathway, were not markedly responsible for the vagal stimulation-mediated cardioprotection observed under our experimental conditions. On the other hand, bradycardia played a significant role in the vagal stimulation-induced cardioprotection against acute myocardial ischemia and reperfusion.

Acknowledgments

This study was supported by a Health and Labor Sciences Research Grant for Research on Advanced Medical Technology, a Health and Labor Sciences Research Grant for Research on Medical Devices for Analyzing, Supporting and Substituting the Function of the Human Body, and a Health and Labor Sciences Research Grant H18-Iryo-Ippan-023 from the Ministry of Health, Labour and Welfare of Japan.

References

Akiyama, T., Yamazaki, T., Ninomiya, I., 1994. In vivo detection of endogenous acetylcholine release in cat ventricles. American Journal of Physiology 266 (3 Pt 2), H854–H860.
Bopassa, J.C., Ferrera, R., Gateau-Roesch, O., Couture-Lepetit, E., Ovize, M., 2006. PI 3-kinase regulates the mitochondrial transition pore in controlled reperfusion and postconditioning. Cardiovascular Research 69 (1), 178–185.
Buck, J.D., Warltier, D.C., Hardman, H.F., Gross, G.J., 1981. Effects of sotalol and vagal stimulation on ischemic myocardial blood flow distribution in the canine heart. The Journal of Pharmacology and Experimental Therapeutics 216 (2), 347–351.
Cheng, Y., George, I., Yi, G.H., Reiken, S., Gu, A., Tao, Y.K., Muraskin, J., Qin, S., He, K.L., Hay, I., Yu, K., Oz, M.C., Burkhoff, D., Holmes, J., Wang, J., 2007. Bradycardic therapy improves left ventricular function and remodeling in dogs with coronary embolization-induced chronic heart failure. The Journal of Pharmacology and Experimental Therapeutics 321 (2), 496–476.
Feigl, E.O., 1969. Parasympathetic control of coronary blood flow in dogs. Circulation Research 25 (5), 509–519.
Feliciano, L., Henning, R.J., 1998. Vagal nerve stimulation releases vasoactive intestinal peptide which significantly increases coronary artery blood flow. Cardiovascular Research 40 (1), 45–55.
Glantz, S.A., 2002. Primer of Biostatistics, 5th ed. McGraw-Hill, New York.
Hausenloy, D.J., Yellon, D.M., 2004. New directions for protecting the heart against ischaemia–reperfusion injury: targeting the reperfusion injury salvage kinase (RISK)-pathway. Cardiovascular Research 61 (3), 448–460.
Henning, R.J., Sawmiller, D.R., 2001. Vasoactive intestinal peptide: cardiovascular effects. Cardiovascular Research 49 (1), 27–37.
Kawada, T., Yamazaki, T., Akiyama, T., Mori, H., Inagaki, M., Shishido, T., Takaki, H., Sugimachi, M., Sunagawa, K., 2002. Effects of brief ischaemia on myocardial acetylcholine and noradrenaline levels in anaesthetized cats. Autonomic Neuroscience: Basic and Clinical 95 (1–2), 37–42.
Kawada, T., Yamazaki, T., Akiyama, T., Li, M., Ariumi, H., Mori, H., Sunagawa, K., Sugimachi, M., 2006. Vagal stimulation suppresses ischemia-induced myocardial interstitial norepinephrine release. Life Sciences 78 (8), 882–887.
Kitagawa, H., Yamazaki, T., Akiyama, T., Sugimachi, M., Sunagawa, K., Mori, H., 2005. Microdialysis separately monitors myocardial interstitial myoglobin during ischemia and reperfusion. American Journal of Physiology. Heart and Circulatory Physiology 289 (2), H924–H930.
Lazdunski, M., Frelin, C., Vigne, P., 1985. The sodium/hydrogen exchange system in cardiac cells: its biochemical and pharmacological properties and its role in regulating internal concentrations of sodium and internal pH. Journal of Molecular and Cellular Cardiology 17 (11), 1029–1042.
Li, M., Zheng, C., Sato, T., Kawada, T., Sugimachi, M., Sunagawa, K., 2004. Vagal nerve stimulation markedly improves long-term survival after chronic heart failure in rats. Circulation 109 (1), 120–124.
Maughan, W.L., Sunagawa, K., Burkhoff, D., Graves Jr., W.L., Hunter, W.C., Sagawa, K., 1985. Effect of heart rate on the canine end-systolic pressure–volume relationship. Circulation 72 (3), 654–659.
Myers, R.W., Pearlman, A.S., Hyman, R.M., Goldstein, R.A., Kent, K.M., Goldstein, R.E., Epstein, S.E., 1974. Beneficial effects of vagal stimulation and bradycardia during experimental acute myocardial ischemia. Circulation 49 (5), 943–947.
Nabutovsky, Y., Florio, J., Morgan, K., Grill, W.M., Farazi, T.G., 2007. Lead design and initial applications of a new lead for long-term endovascular vagal stimulation. Pacing and Clinical Electrophysiology 30 (11), S215–S218.
Nakayama, Y., Miyano, H., Shishido, T., Inagaki, M., Kawada, T., Sugimachi, M., Sunagawa, K., 2001. Heart rate-independent vagal effect on end-systolic elastance of the canine left ventricle under various levels of sympathetic tone. Circulation 104 (19), 2277–2279.
Oldenburg, O., Critz, S.D., Cohen, M.V., Downey, J.M., 2003. Acetylcholine-induced production of reactive oxygen species in adult rabbit ventricular myocytes is dependent on phosphatidylinositol 3- and Src-kinase activation and mitochondrial K_{ATP} channel opening. Journal of Molecular and Cellular Cardiology 35 (6), 653–660.
Piper, H.M., 1989. Energy deficiency, calcium overload or oxidative stress: possible causes of irreversible ischemic myocardial injury. Klinische Wochenschrift 67 (9), 465–476.

Piper, H.M., Abdallah, Y., Schäfer, C., 2004. The first minutes of reperfusion: a window of opportunity for cardioprotection. Cardiovascular Research 61 (3), 365–371.
Przyklenk, K., Kloner, R.A., 1995. Low-dose i.v. acetylcholine acts as a "preconditioning-mimetic" in the canine model. Journal of Cardiac Surgery 10 (4), 389–395.
Qin, Q., Downey, J.M., Cohen, M.V., 2003. Acetylcholine but not adenosine triggers preconditioning through PI3-kinase and a tyrosine kinase. American Journal of Physiology. Heart and Circulatory Physiology 284 (2), H727–H734.
Reid, J.V.O., Ito, B.R., Huang, A.H., Buffington, C.W., Feigl, E.O., 1985. Parasympathetic control of transmural coronary blood flow in dogs. American Journal of Physiology 249 (2 Pt 2), H337–H343.
Rosenshtraukh, L., Danilo Jr., P., Anyukhovsky, E.P., Steinberg, S.F., Rybin, V., Brittain-Valenti, K., Molina-Viamonte, V., Rosen, M.R., 1994. Mechanisms for vagal modulation of ventricular repolarization and of coronary occlusion-induced lethal arrhythmias in cats. Circulation Research 75 (4), 722–732.
Sammel, N.L., Norris, R.M., Hughes, C.F., Johnson, R.N., Ashton, N.G., Elliott, R.L., 1983. Severity of canine myocardial infarcts in relation to indices of oxygen demand: preservation of myocardial creatine kinase activity by vagal stimulation and propranolol. Cardiovascular Research 17 (1), 50–60.
Shinke, T., Takeuchi, M., Takaoka, H., Yokoyama, M., 1999. Beneficial effects of heart rate reduction on cardiac mechanics and energetics in patients with left ventricular dysfunction. Japanese Circulation Journal 63 (12), 957–964.
Takami, H., Matsuda, H., Kuki, S., Nishimura, M., Kawashima, Y., Watari, H., Furuya, E., Tagawa, K., 1990. Leakage of cytoplasmic enzymes from rat heart by the stress of cardiac beating after increase in cell membrane fragility by anoxia. Pflügers Archiv 416 (1–2), 144–150.
Vanoli, E., de Ferrari, G.M., Stramba-Badiale, M., Hull Jr., S.S., Foreman, R.D., Schwartz, P.J., 1991. Vagal stimulation and prevention of sudden death in conscious dogs with a healed myocardial infarction. Circulation Research 68 (5), 1471–1481.
Wienen, W., Kammermeier, H., 1988. Intra- and extracellular markers in interstitial transudate of perfused rat hearts. American Journal of Physiology 254 (4 Pt 2), H785–H794.
Young, L.H., Ikeda, Y., Scalia, R., Lefer, A.M., 2000. Wortmannin, a potent antineutrophil agent, exerts cardioprotective effects in myocardial ischemia/reperfusion. The Journal of Pharmacology and Experimental Therapeutics 295 (1), 37–43.

Am J Physiol Heart Circ Physiol 295: H1081–H1089, 2008.
First published June 27, 2008; doi:10.1152/ajpheart.00023.2008.

Muscle mechanoreflex augments arterial baroreflex-mediated dynamic sympathetic response to carotid sinus pressure

Kenta Yamamoto,[1,2] Toru Kawada,[2] Atsunori Kamiya,[2] Hiroshi Takaki,[2] Toshiaki Shishido,[2] Kenji Sunagawa,[3] and Masaru Sugimachi[2]

[1]*Consolidated Research Institute for Advanced Science and Medical Care, Waseda University, Tokyo;* [2]*Department of Cardiovascular Dynamics, Advanced Medical Engineering Center, National Cardiovascular Center Research Institute, Osaka; and* [3]*Department of Cardiovascular Medicine, Graduate School of Medical Sciences, Kyushu University, Fukuoka, Japan*

Submitted 8 January 2008; accepted in final form 19 June 2008

Yamamoto K, Kawada T, Kamiya A, Takaki H, Shishido T, Sunagawa K, Sugimachi M. Muscle mechanoreflex augments arterial baroreflex-mediated dynamic sympathetic response to carotid sinus pressure. *Am J Physiol Heart Circ Physiol* 295: H1081–H1089, 2008. First published June 27, 2008; doi:10.1152/ajpheart.00023.2008.—Although the muscle mechanoreflex is one of the pressor reflexes during exercise, its interaction with dynamic characteristics of the arterial baroreflex remains to be quantitatively analyzed. In anesthetized, vagotomized, and aortic-denervated rabbits ($n = 7$), we randomly perturbed isolated carotid sinus pressure (CSP) using binary white noise while recording renal sympathetic nerve activity (SNA) and arterial pressure (AP). We estimated the transfer functions of the baroreflex neural arc (CSP to SNA) and peripheral arc (SNA to AP) under conditions of control and muscle stretch of the hindlimb (5 kg of tension). The muscle stretch increased the dynamic gain of the neural arc while maintaining the derivative characteristics [gain at 0.01 Hz: 1.0 ± 0.2 vs. 1.4 ± 0.6 arbitrary units (au)/mmHg, gain at 1 Hz: 1.7 ± 0.6 vs. 2.7 ± 1.4 au/mmHg; $P < 0.05$, control vs. stretch]. In contrast, muscle stretch did not affect the peripheral arc. In the time domain, muscle stretch augmented the steady-state response at 50 s (−1.1 ± 0.3 vs. −1.7 ± 0.7 au; $P < 0.05$, control vs. stretch) and negative peak response (−2.1 ± 0.5 vs. −3.1 ± 1.5 au; $P < 0.05$, control vs. stretch) in the SNA step response. A simulation experiment using the results indicated that the muscle mechanoreflex would accelerate the closed-loop AP regulation via the arterial baroreflex.

muscle stretch; transfer function; exercise pressor reflex; exercise; arterial pressure

THE ARTERIAL BAROREFLEX SYSTEM plays an important role in stabilizing arterial pressure (AP) during daily activity. Knowledge of the open-loop static and dynamic characteristics of the arterial baroreflex is essential for a systematic understanding of how the baroreflex system regulates AP. The static characteristics provide information on the operating point of the baroreflex system (19, 34, 48), whereas the dynamic characteristics determine the stability and quickness of the baroreflex system (14, 22, 23). Importantly, many previous studies showed that exercise resets the baroreflex function (3, 5, 6, 29, 30, 32, 35, 36, 40, 45, 47). However, only a few investigations focused on the dynamic characteristics of the arterial baroreflex during exercise (10, 36, 38, 57). The dynamic characteristics of the arterial baroreflex determine how quickly or slowly the system would response to baroreceptor pressure perturbations. Such information cannot be obtained from the static characteristics alone.

The neural mechanisms responsible for changes in the baroreflex function during exercise are considered to be mediated by central command (6, 13, 29, 39, 46) and by afferent inputs from metabolic and mechanical-sensitive skeletal muscle receptors (11, 12, 17, 41, 43, 44, 49). Regarding the static interaction between the muscle mechanoreflex and arterial baroreflex, we performed a baroreflex open-loop study and reported that muscle stretch extended the response range of sympathetic nerve activity (SNA) to baroreceptor pressure input (58, 59). Based on the results, we hypothesized that the activation of the muscle mechanoreflex would augment the dynamic SNA response to baroreceptor pressure input under open-loop conditions. To the best of our knowledge, however, the effects of the muscle mechanoreflex on the dynamic characteristics of the arterial baroreflex have never been reported.

To test the above hypothesis, we identified the dynamic characteristics of the baroreflex during muscle stretch in anesthetized rabbits under baroreflex open-loop conditions (14, 22, 23). The transfer functions from baroreceptor pressure input to SNA (the baroreflex neural arc) and from SNA to AP (the baroreflex peripheral arc) were estimated by a white noise approach (51). The "whiteness" is essential for the system identification of the arterial baroreflex because it is equivalent mathematically to test the system with all possible pressure changes within the frequency range of interest.

METHODS

Surgical preparations. Animals were cared for in strict accordance with the Guiding Principles for the Care and Use of Animals in the Field of Physiological Sciences approved by the Physiological Society of Japan. All protocols were approved by the Animal Subjects Committee of the National Cardiovascular Center. Seven Japanese White rabbits weighing 2.6–3.0 kg were anesthetized via an intravenous injection (2 ml/kg) of a mixture of urethane (250 mg/ml) and α-chloralose (40 mg/ml) and were mechanically ventilated with oxygen-enriched room air. Supplemental anesthetics (0.2–0.3 $ml \cdot kg^{-1} \cdot h^{-1}$) were administered continuously to maintain stable AP and heart rate levels during intervals of experimental protocols, which were indicative of an appropriate level of anesthesia. Arterial blood was sampled from the left common carotid artery. Rabbits were slightly hyperventilated to suppress chemoreflexes (arterial P_{CO_2} ranged from 30 to 35 mmHg, arterial $P_{O_2} > 300$ mmHg). Arterial blood pH was within the

Address for reprint requests and other correspondence: K. Yamamoto, Consolidated Research Institute for Advanced Science and Medical Care, Waseda Univ., 513 Wasedatsurumakicho, Shinjuku, Tokyo 162-0041, Japan (e-mail: kenta@aoni.waseda.jp).

The costs of publication of this article were defrayed in part by the payment of page charges. The article must therefore be hereby marked "*advertisement*" in accordance with 18 U.S.C. Section 1734 solely to indicate this fact.

physiological range when examined at the end of the surgical preparation as well as at the end of the experiment. The body temperature of each animal was maintained at ~38°C with a heating pad. AP was measured using a high-fidelity pressure transducer (Millar Instruments, Houston, TX) inserted from the right femoral artery to the aortic arch.

We isolated bilateral carotid sinuses from the systemic circulation by ligating the internal and external carotid arteries and other small branches originating from the carotid sinus region. Isolated carotid sinuses were filled with warmed physiological saline via catheters inserted through the common carotid arteries. Intra-CSP was controlled by a servo-controlled piston pump (model ET-126A, Labworks, Costa Mesa, CA). Bilateral vagal and aortic depressor nerves were sectioned at the neck to minimize reflexes from the cardiopulmonary region and from the aortic arch.

We exposed the left renal sympathetic nerve retroperitoneally and attached a pair of stainless steel wire electrodes (Bioflex wire AS633, Cooner Wire, Chatsworth, CA) to record SNA. The nerve bundle peripheral to the electrodes was tightly ligated and crushed to eliminate afferent signals from the kidney. The nerve and electrodes were secured with silicone glue (Kwik-Sil, World Precision Instruments, Sarasota, FL). The preamplified nerve signal was band-pass filtered at 150–1,000 Hz, full-wave rectified, and low-pass filtered with a cutoff frequency of 30 Hz to quantify the nerve activity.

With the rabbit in the prone position, the sacrum, left ankle, and knee were clamped with a custom-made apparatus to prevent body trunk and hindlimb movement during muscle stretch. The left triceps surae muscle, Achilles tendon, and calcaneus bone were exposed. The left triceps surae muscle was isolated from the surrounding tissue. The Achilles tendon was severed from the calcaneus bone and attached to a force transducer (Load Cell LUR-A-SA1, Kyowa Electronic Instruments, Tokyo, Japan). During muscle stretch, the other side of the force transducer was connected to a 5-kg weight via a pulley.

Protocols. To obtain operating pressure values, the carotid sinus baroreflex negative feedback loop was effectively closed by adjusting CSP to AP. Mean AP (and thus mean CSP) at steady state was treated as the operating pressure under control conditions. We then performed muscle stretch for 1 min while the carotid sinus baroreflex was effectively closed. Mean AP during the last 10 s of muscle stretch was treated as the operating pressure under muscle stretch conditions.

To estimate the baroreflex dynamic characteristics, CSP was assigned either high (+20 mmHg) or low (−20 mmHg) pressure values around the operating pressure according to a binary white noise sequence. The switching interval of the binary white noise signal was set at 500 ms so that the CSP power spectrum was fairly flat up to 1 Hz. We confirmed that the muscle stretch produced a sustained SNA increase for at least 7 min (58). To limit the maximum duration of muscle stretch within this time period, a 6-min CSP perturbation was performed twice using different binary sequences, and the two sets of data were pooled for analyses under both control and muscle stretch conditions. The order of control and muscle stretch conditions was randomized across the animals.

Data analysis. We recorded CSP, muscle tension, SNA, and AP at a sampling rate of 200 Hz using a 12-bit analog-to-digital converter. Data were stored on a dedicated laboratory computer system.

To estimate the neural arc transfer function of the carotid sinus baroreflex, we treated CSP as the input and SNA as the output of the system. In the peripheral arc transfer function, we treated SNA as the input and AP as the output of the system. In the total loop transfer function, we treated CSP as the input and AP as the output of the system. Data analysis was started from 90 s after the initiation of each trial to process the stationary portion of data without the effects of transition from closed-loop CSP waveform to open-loop binary white noise CSP input and the transition from nonstretch to stretch of muscle mechanoreceptors. The input-output data pairs were resampled at 10 Hz and segmented into 50%-overlapping bins of 1,024 points each. For each segment, a linear trend was subtracted, and a Hanning window was applied. A fast Fourier transform was performed to obtain the frequency spectra of the input and output signals. The ensemble averages of input power spectral density [$S_{XX}(f)$], output power spectral density [$S_{YY}(f)$], and cross-spectral density between the input and output [$S_{YX}(f)$] were obtained over eight segments derived from two sets of data, where f represents frequency. Finally, we calculated the transfer function from input to output [$H(f)$] using the following equation (27):

$$H(f) = \frac{S_{YX}(f)}{S_{XX}(f)} \quad (1)$$

Hereinafter, we denote the modulus as the dynamic gain of the transfer function. To quantify the linear dependence between input and output signals in the frequency domain, we calculated a magnitude-squared coherence function [Coh(f)] using the following equation (27):

$$\mathrm{Coh}(f) = \frac{|S_{YX}(f)|^2}{S_{XX}(f)S_{YY}(f)} \quad (2)$$

The coherence value ranges from zero to unity. Unity coherence indicates perfect linear dependence between input and output signals, whereas zero coherence indicates total independence between the two signals.

To facilitate an intuitive understanding of the transfer function, the step response corresponding to the transfer function was also calculated as follows. The system impulse response was derived from the inverse Fourier transform of $H(f)$. The step response was obtained from the time integral of the impulse response.

Statistical analysis. All data are presented as means ± SD. Because the amplitude of SNA varied depending on recording conditions, such as the physical contact between the nerve and electrodes, SNA was presented in arbitrary units (au). Neural and peripheral arc transfer functions were normalized in each animal so that the average gain values below 0.03 Hz in the control trial became unity. To compare the transfer functions between two conditions, a transfer gain value at 0.01 Hz ($G_{0.01}$), 0.1 Hz ($G_{0.1}$), 0.5 Hz ($G_{0.5}$), and 1 Hz (G_1) were calculated. In the step response of the neural arc, the steady-state step response at 50 s (S_{50}), the negative peak value (S_{peak}), and the time to negative peak (T_{peak}) were calculated. The effects of muscle stretch on these parameters were examined using the paired t-test. Differences were considered significant when $P < 0.05$.

RESULTS

Figure 1 shows a typical time series of CSP, muscle tension, SNA, and AP under control (*left*) and muscle stretch (*right*) conditions. Although the same binary sequence was applied for two conditions in each animal, different binary sequences were applied for different animals to reduce possible systematic errors in system identification caused by a bias in whiteness specific to a selected binary sequence. The mean CSP during muscle stretch conditions (Fig. 1, *right*) was set higher than that during the control conditions (Fig. 1, *left*) to mimic the increase in the operating pressure during muscle stretch under baroreflex closed-loop conditions (i.e., the AP increase by muscle stretch increases the mean input pressure to the baroreceptors) . Muscle stretch increased mean levels of SNA and AP compared with control conditions during the experiment (Table 1).

Figure 2 shows the transfer functions of the neural (*left*) and peripheral (*right*) arcs estimated under the control and muscle stretch conditions; gain plots (*top*), phase plots (*middle*), and Coh(f) (*bottom*) are also presented. The thin and thick solid lines in Fig. 2 indicate control and muscle stretch conditions, respectively. In the neural arc, the dynamic gain increased as

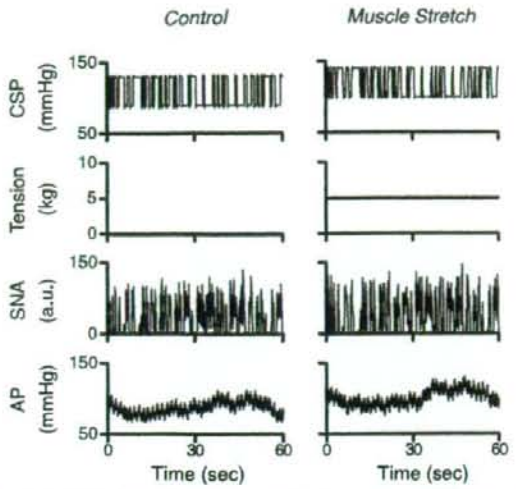

Fig. 1. Typical time series of intracarotid sinus pressure (CSP), muscle tension, sympathetic nerve activity [SNA; in arbitrary units (au)], and arterial pressure (AP) under control (*left*) and muscle stretch (*right*) conditions. CSP was perturbed according to a binary white noise sequence. Muscle stretch increased mean levels of SNA and AP under muscle stretch conditions compared with the control conditions.

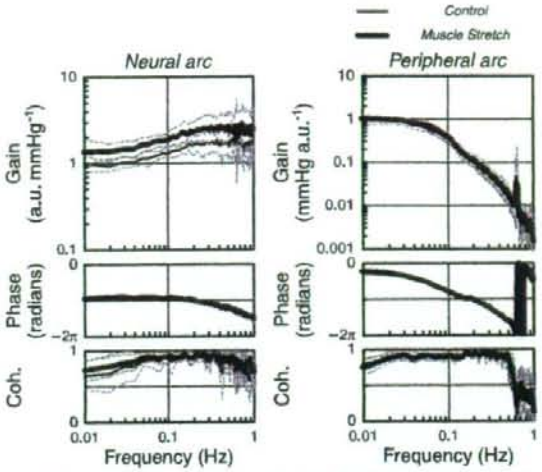

Fig. 2. Transfer functions of the neural (*left*) and peripheral (*right*) arcs under control and muscle stretch conditions. In the neural arc, the input was CSP and the output was SNA. In the peripheral arc, the input was SNA and the output was AP. The mean level of CSP input to the neural arc was set higher under muscle stretch conditions than under control conditions to mimic the physiological condition (i.e., baroreflex closed-loop conditions). Gain plots (*top*), phase plots (*middle*) and coherence (Coh) functions (*bottom*) are shown. Thin and thick solid lines indicate control and muscle stretch conditions, respectively. In the neural arc (*left*), muscle stretch caused an approximately parallel upward shift of the gain plot. Solid and dashed lines represent means and means ± SD values, respectively.

the frequency of input modulation increased under both conditions, indicating derivative characteristics of the neural arc. Muscle stretch caused an approximately parallel upward shift of the gain plot. The phase approached $-\pi$ radians ($-180°$) at the lowest frequency (0.01 Hz) under both conditions, reflecting the negative feedback character of the baroreflex neural arc (i.e., an increase in CSP decreased SNA). Phase plots were nearly superimposed between the two conditions. Coherence values did not differ between both conditions. In the peripheral arc, the dynamic gain decreased in the frequency range from 0.05 to 1 Hz as the frequency of input modulation increased under both conditions, indicating the low-pass characteristics of the peripheral arc. The phase approached 0 radians at the lowest frequency (0.01 Hz) under both conditions, reflecting the fact that an increase in SNA increased AP. The phase lagged with increasing frequency up to 1 Hz. The gain plot, phase plot, and Coh(f) did not differ between both conditions.

Table 1. *Mean levels and CVs of CSP, SNA, and AP at 1, 2, 4, and 6 min under control and muscle stretch conditions*

	Time			
	1 min	2 min	4 min	6 min
		CSP		
Control	95±18	96±18	95±18	96±18
CV	13±2	12±3	11±3	14±2
Muscle stretch	114±15*	115±16*	113±16*	114±15*
CV	11±2	11±1	10±2	12±2
		SNA		
Control	102±4	99±5	100±4	99±4
CV	46±11	45±9	43±9	47±9
Muscle stretch	133±22*	129±21*	127±17*	126±17*
CV	48±11	47±8	44±9	49±10
		AP		
Control	90±21	89±20	88±16	88±18
CV	7±2	6±2	6±2	6±2
Muscle stretch	107±26*	105±22*	104±15*	101±15*
CV	7±3	6±3	6±3	7±2

Values are means ± SD; $n = 7$. CSP, carotid sinus pressure (in mmHg); SNA, sympathetic nerve activity (in %); AP, arterial pressure (in mmHg); CV, coefficient of variation. Mean and CV values were calculated from 30-s data ending at each time point. *$P < 0.05$ vs. control.

Table 2 summarizes gains of the transfer functions. In the neural arc, $G_{0.01}$, $G_{0.1}$, $G_{0.5}$, and G_1 were higher under muscle

Table 2. *Gains of the transfer functions*

	Control	Muscle Stretch
Neural arc		
$G_{0.01}$, au/mmHg	1.01±0.23	1.44±0.56*
$G_{0.1}$, au/mmHg	1.30±0.11	1.86±0.37*
$G_{0.5}$, au/mmHg	1.77±0.64	2.65±1.08*
G_1, au/mmHg	1.72±0.66	2.72±1.40*
Peripheral arc		
$G_{0.01}$, mmHg/au	1.08±0.06	1.06±0.20
$G_{0.1}$, mmHg/au	0.37±0.09	0.42±0.09
$G_{0.5}$, mmHg/au	0.02±0.01	0.02±0.01
G_1, mmHg/au	0.004±0.001	0.004±0.002
Total loop		
$G_{0.01}$, mmHg/mmHg	1.08±0.18	1.53±0.63*
$G_{0.1}$, mmHg/mmHg	0.48±0.12	0.81±0.31*
$G_{0.5}$, mmHg/mmHg	0.04±0.04	0.06±0.04*
G_1, mmHg/mmHg	0.006±0.003	0.013±0.013

Values are means ± SD; $n = 7$. $G_{0.01}$, $G_{0.1}$, $G_{0.5}$, and G_1, dynamic gains at 0.01, 0.1, 0.5, and 1 Hz, respectively; au, arbitrary units. *$P < 0.05$ vs. control.

stretch compared with control conditions. In the peripheral arc, $G_{0.01}$, $G_{0.1}$, $G_{0.5}$, and G_1 were unchanged between control and muscle stretch conditions.

Figure 3 shows the total baroreflex loop transfer functions (CSP to AP) under control and muscle stretch conditions. The thin and thick solid lines in Fig. 3 indicate control and muscle stretch conditions, respectively. The dynamic gain decreased as the frequency of input modulation increased under both conditions, indicating low-pass characteristics. The dynamic gain under muscle stretch conditions was higher than that under control conditions in frequency from 0.01 to 0.5 Hz (Table 2). The phase plot and Coh(f) did not differ between both conditions.

Figure 4 shows step responses of SNA corresponding to the transfer functions in the neural arc shown in Fig. 2. The initial drop in the SNA response as well as the steady-state response was augmented during muscle stretch (Table 3). T_{peak} did not differ between control and muscle stretch conditions (Table 3).

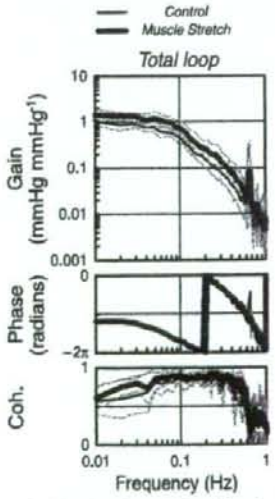

Fig. 3. Total loop transfer functions from CSP to AP under control and muscle stretch conditions. Gain plots (*top*), phase plots (*middle*) and coherence functions (*bottom*) are shown. Thin and thick solid lines indicate control and muscle stretch conditions, respectively. The dynamic gain decreased as the frequency of input modulation increased under both conditions, indicating low-pass characteristics. Muscle stretch caused an approximately parallel upward shift of the gain plot. Solid and dashed lines represent means and means ± SD values, respectively.

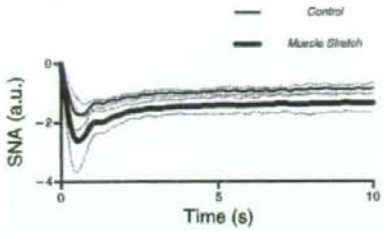

Fig. 4. Step responses corresponding to transfer functions of the neural arc obtained from Fig. 2, showing the SNA response to a 1-mmHg increase in input pressure. Thin and thick solid lines indicate control and muscle stretch conditions, respectively. The initial drop in the SNA response as well as the steady-state response was augmented by the muscle stretch. Solid and dashed lines represent means and means ± SD values, respectively.

DISCUSSION

The key new findings of the present study are as follows. Muscle stretch increased the dynamic gain of the carotid sinus baroreflex neural arc as estimated by binary white noise input (Fig. 2). In contrast, the peripheral arc transfer function remained unchanged irrespective of the muscle stretch (Fig. 2). These results suggest that during muscle mechanoreflex activation, the dynamic SNA response to CSP perturbation is augmented.

System identification by the white noise approach. To identify the dynamic characteristics of arterial baroreflex function quantitatively, we described the carotid sinus baroreflex control of SNA and AP in terms of system identification using the white noise technique. Compared with the traditional approach of testing dynamic properties of the physiological system with step and sine wave stimuli, the white noise approach has definite advantages, as follows (27). First, if a step stimulus is applied, we learn the response of the system to this step and have little notion of the response of the system to any other type of stimulus. If a sinusoidal pulse is applied, then we know the response of the system to such a stimulus and little else. The same applies for any other specific waveform. Theoretically speaking, the system is tested with every possible stimulus in the white noise approach. The white noise stimulus is a very rich stimulus. It should be emphasized that the white noise method is perfectly suited to the analysis of linear systems. As shown in Figs. 2 and 3, high coherence values close to unity indicate the validity of our method for system identification. Second, the identification of the physiological system through the white noise technique is largely unaffected by the types of contaminating noise usually present in such a system. Our study provides the first and quantitative description of the dynamic characteristics of the carotid sinus baroreflex during isolated activation of mechanosensitive afferents from skeletal muscle.

Effects of the muscle mechanoreflex on dynamic characteristics of the carotid sinus baroreflex. The effects of activation of afferents from skeletal muscle, such as those occurring during exercise, on the arterial baroreflex have been extensively studied (5, 13, 29, 42, 43, 49, 58, 59). These studies have demonstrated that the afferent input from muscle resets the baroreflex control of AP, heart rate, and SNA. However, the dynamic characteristics of the arterial baroreflex during isolated activation of muscle mechanosensitive afferents have never been analyzed. In the present study, muscle stretch increased dynamic gain in every frequency (Fig. 2 and Table

Table 3. *Parameters of step responses*

	Control	Muscle Stretch
S_{50}, au	−1.05±0.30	−1.69±0.69*
S_{peak}, au	−2.10±0.50	−3.08±1.45*
T_{peak}, s	0.63±0.21	0.64±0.20

Values are means ± SD; n = 7. A step response is defined as a SNA response to a 1-mmHg change in input pressure. S_{50}, step response at 50 s; S_{peak}, negative peak response; T_{peak}, time to negative peak. *$P < 0.05$ vs. control.

2), whereas it did not affect the peripheral arc. These data are the first to provide quantitative evidence demonstrating that the dynamic SNA response to CSP perturbation is augmented during isolated activation of the muscle mechanoreflex. Although an increase in dynamic gain in the lowest frequency (0.01 Hz) was expected from the results of our previous studies showing an increase in static gain by muscle stretch (58, 59), the information was insufficient to perform a simulation study to examine the effects of muscle stretch on the closed-loop dynamic AP regulation (see *Physiological implications*). The present study extended our previous work by providing additional information on the dynamic interaction over a wide range of frequencies between 0.01 and 1 Hz in the carotid sinus baroreflex.

The static characteristics of the arterial baroreflex determine an operating point of the baroreflex system. Furthermore, the static characteristics described by a modeled sigmoid function provide the parameters of threshold, saturation, and maximal gain at the centering point. However, the static characteristics alone cannot provide the information on the changes over time in the response of the baroreflex system. On the other hand, dynamic analysis techniques such as transfer function analysis estimated by the white noise approach provide information on the stability and quickness of the system response. The dynamic SNA response to baroreceptor pressure input became greater as the frequency of input modulation increased, suggesting derivative characteristics (i.e., high-pass characteristics) of the baroreflex neural arc (Fig. 2, *left*, thin solid line). In contrast, the dynamic AP response to SNA became smaller as the frequency of SNA modulation increased, indicating low-pass characteristics of the baroreflex peripheral arc (Fig. 2, *right*, thin solid line). The total loop transfer function (CSP to AP) is determined by a product of the neural and peripheral arc transfer functions (Fig. 3, thin solid line). Therefore, the decreasing slope of dynamic gain in the total loop transfer function was shallower than that in the corresponding peripheral arc. In other words, the fast neural arc effectively compensates for the slow peripheral arc to accelerate dynamic AP regulation by the baroreflex negative-feedback loop (14). During muscle stretch, the dynamic gain in the neural arc was increased by ~50% in every frequency under study (Fig. 2 and Table 2), indicating that the derivative characteristics of the neural arc were maintained. As a result, the effect of the neural arc compensating for the slow AP response was preserved during the activation of muscle mechanoreflex (Fig. 3 and Table 2). Furthermore, the total loop dynamic gain was augmented during the muscle stretch due to the upward shift of the neural arc transfer function.

Because we used passive muscle stretch as the input for the muscle mechanoreflex, the physiological significance of the present results should be interpreted carefully. Several studies have examined the arterial baroreflex control of SNA during static and dynamic exercise. Static and heavy dynamic exercise resets the baroreflex control of SNA to higher SNA levels with an increase in its sensitivity (9, 11, 17, 32). On the other hand, mild to moderate dynamic exercise resets the baroreflex control of SNA without any change in its sensitivity (3, 24, 38). Because the muscle mechanoreflex is activated during mild to moderate dynamic exercise (4), our results indicate that the muscle mechanoreflex may contribute to increasing the baroreflex gain of SNA during mild to moderate dynamic exercise. In addition to differences in the measured SNA (renal vs. muscle), analytic methods of baroreflex function, modes of mechanoreflex activation, and/or species between the present study and previous studies, the cardiopulmonary baroreflex should be taken into account. Charkoudian et al. (1) demonstrated that increasing central venous pressure via head-down tilt or saline infusion attenuated the baroreflex sensitivity in the control of SNA. The activation of cardiopulmonary baroreceptors induced by increasing central venous pressure may influence the arterial baroreflex control during dynamic exercise (37). In the present study, however, the cardiopulmonary baroreflex did not operate due to bilateral vagotomy.

Previous studies (7, 25) have suggested that the muscle mechanoreflex has a dominant role in pressor reflexes during muscle contraction in anesthetized or decerebrate cats. Although we believe that the mechanoreflex is one of the pressor reflexes during exercise, the functional importance of the muscle mechanoreflex in cardiovascular regulation during exercise in conscious conditions is debatable. Matsukawa et al. (28) recently reported that blockade of the muscle mechanoreflex by gadolinium did not alter AP responses to isometric exercise in conscious cats. Moreover, they found that gadolinium significantly diminished the pressor responses to passive muscle stretch in anesthetized cats. These observations suggest that, under the experimental design, the muscle mechanoreflex would not be activated during exercise or, even if it was activated, it has no functional importance in cardiovascular responses to exercise in conscious conditions. One criticism for the study is that there is always a possibility that changes in the central command in conscious conditions had compensated for the lack of muscle mechanoreflex. Further studies are needed to better understand the role of the muscle mechanoreflex on neural cardiovascular responses during exercise.

High-pass characteristics of the baroreflex neural arc. It is likely that the dynamic characteristics of the baroreflex neural arc actually reflect the intrinsic and synaptic properties of central nervous system neurons and neural circuits that transmit baroreceptor input. However, the central baroreceptor synapses are characterized as a low-pass filter (26). The difference between high-pass characteristics of the neural arc transfer gain and low-pass characteristics of the central baroreceptor synaptic transmission could be attributable to the difference of estimated frequency ranges. Frequency-dependent depression (FFD) of synaptic transmission in the baroreflex central pathways is the phenomenon that the probability of excitatory postsynaptic potentials progressively reduces as the frequency of afferent input increases beyond 1 Hz (2, 33). Although FDD and transfer gain should be discriminated in theory, interactions between FDD and transfer gain may occur when the modulation frequency of afferent fiber stimulation approached the frequency range of FDD. Indeed, Kawada et al. (23) found high-cut characteristics of the baroreflex neural arc in the frequency range above ~1 Hz. In the present study, the transfer gain was derived from 0.01 to 1 Hz. Whether the dynamic interaction between carotid sinus baroreflex and muscle mechanoreflex exists in the frequency range beyond 1 Hz awaits further studies.

Part of the high-pass characteristics in the baroreflex neural arc is attributable to the derivative nature observed in the baroreceptor transduction from CSP input to baroreceptor afferent nerve activity (i.e., mechanoneural transduction) (21).

However, we think there exists high-pass characteristics in the transduction from baroreceptor afferent input to efferent SNA, because the magnitude of high-pass characteristics slightly differs between cardiac and renal SNAs in response to the same baroreceptor pressure perturbation (18).

In an electrical circuit, we can design a high-pass filter only from low-pass filter elements using a feedback loop (Fig. 5). Although the main forward path of the baroreflex neural arc from afferent nerve activity to efferent SNA is considered to be the nucleus tructus solitarius, caudal ventrolateral medulla, and rostral ventrolateral medulla (53), there could be feedback connections between these areas. Therefore, it is possible that synaptic connection has basically low-pass characteristics, whereas the baroreflex neural arc reveals high-pass characteristics as a neural circuit. The speculation also needs to be verified experimentally in the future.

Physiological implications. Under physiological conditions, the baroreflex is closed as a negative feedback system. In the following discussion, we will focus on the effect of the augmentation of dynamic SNA modulation in the neural arc on the closed-loop dynamic AP regulation. Figure 6*A* illustrates a simulator consisting of the linear neural arc transfer function (H_N) and linear peripheral arc transfer function (H_P) followed by the nonlinear sigmoidal components (see the APPENDIX for details). A closed-loop AP response to a stepwise pressure perturbation (−40 mmHg) with pulsatile pressure was simulated, and the result is shown in Fig. 6*B*. Muscle stretch shortened the time to 95% of steady state by ~33% from 7.2 to 4.8 s (shaded and solid arrows in Fig. 6*B*). This result suggests that, under baroreflex closed-loop conditions, the rate of recovery in AP following a pressure perturbation occurs sooner when accompanied by the muscle mechanoreflex. Increasing the quickness of the negative-feedback system can be caused by augmentation and/or acceleration of the open-loop transfer function of the system. In our baroreflex open-loop experiment, S_{50} and S_{peak} in the step responses of SNA were augmented by the muscle stretch (Fig. 4 and Table 3). On the other hand, T_{peak} did not differ between control and muscle stretch conditions (Fig. 4 and Table 3). These results suggest that the improvement in the quickness of the AP restoration via the baroreflex observed in the closed-loop simulation was induced by augmentation, rather than acceleration, of the dynamic SNA response in the neural arc. However, further experimental studies are needed to verify the simulation model.

Limitations. The present study has several limitations. First, we performed the experiment in anesthetized animals. Previous studies have suggested that any anesthetic could alter the baroreflex regulation in AP (54–56). The gain of the baroreflex is reported in the conscious state to be higher (~2-fold) than in the anesthetized state. A previous study (52) suggested that α-chloralose anesthesia could alter the dynamic characteristics of the baroreflex regulation around the frequency of 5 Hz. However, the anesthesia was convenient for the elimination of the central command. Furthermore, we compared the baroreflex gain between muscle stretch and nonstretch conditions both under anesthesia. Therefore, a reasonable interpretation would be that the increased baroreflex gain is attributable to muscle stretch in this experiment.

Second, stretching of skeletal muscle provides a stimulus for the activation of mechanoreceptors that is different from that which occurs during muscle contraction. During contraction, mechanoreceptors are activated by a shortening of skeletal muscle and by compression of the receptors. Thus, mechanoreceptors may be stimulated in a very different manner during stretch, which would likely affect the magnitude of the corresponding reflex response. In addition, the level of muscle stretch used in our experiment was relatively high (50). The stretch may activate different afferents than contraction (8). Furthermore, the discharge profile of mechanosensitive afferents adapt during static muscle stretch (31). Accordingly, during the muscle stretch for 6 min in the present study, the firing level from the mechanoreceptors might have been

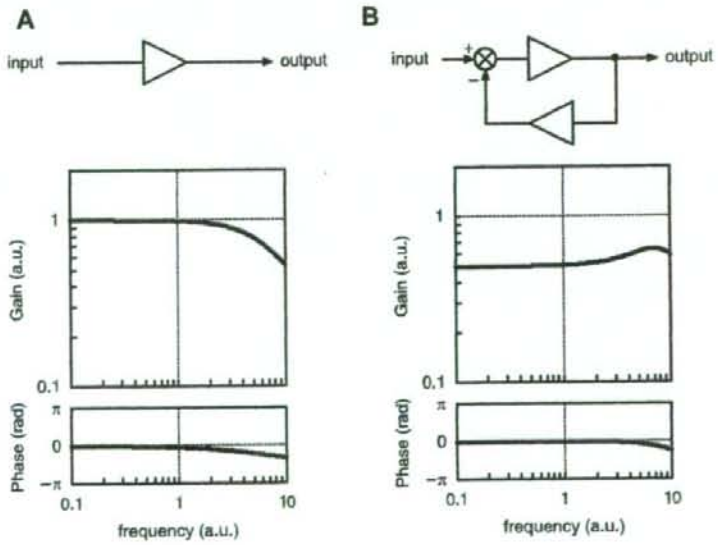

Fig. 5. An example that a circuit consisting of only low-pass elements yields high-pass characteristics as a circuit. *A*: block diagram of a single low-pass element (triangle) and its transfer function. Units for gain and frequency are arbitrary. *B*: block diagram of a circuit with a negative feedback loop with the same low-pass element (triangles). Because gain in the lower frequency range is attenuated more by the low-pass characteristics of the feedback path, the transfer function from input to output reveals high-pass characteristics.

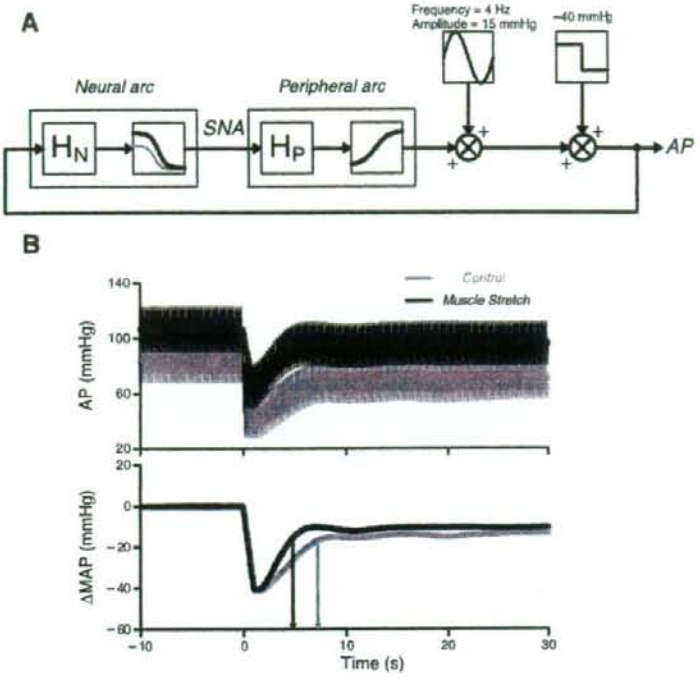

Fig. 6. *A*: simulator of the baroreflex system during activation of the muscle mechanoreflex. A stepwise perturbation with pulsatile pressure was applied to the baroreflex negative feedback system (see the APPENDIX for details). H_N, neural arc transfer function; H_P, peripheral arc transfer function. *B*: simulation results of the closed-loop AP response to the stepwise pressure perturbation (−40 mmHg). Muscle stretch shortened the time to 95% of steady state by −33% (shaded and solid arrows). Shaded and solid thick lines indicate mean AP (MAP) resampled at 1 Hz. ΔMAP, change in MAP from baseline.

steadily diminishing. In fact, the increase in SNA and AP induced by muscle stretch gradually decreased from 90 s to 6 min after the initiation of the muscle stretch, which was used for data analysis (Table 1). However, SNA and AP remained significantly higher under muscle stretch conditions than control conditions over the protocol for 6 min. Thus, we believe that the mechanoreflex remained activated in this protocol. Further studies are required to elucidate the dynamic interactions between baroreflex and mechanoreflex induced by different modes of activation, such as cyclic activation of the mechanoreflex.

Third, the transfer function analysis is useful in identifying the linear input-output relationship of the baroreflex at a given operating point. However, the transfer function cannot characterize the nonlinear input-output relationship of the system. In the presence of nonlinear system behavior such as the baroreflex system, the transfer function analysis is partly compromised, indicating that the absolute output values of the nonlinear system to given input signals cannot be predicted accurately by the transfer function alone. Combining a linear transfer function with a nonlinear sigmoidal element would increase the accuracy to reproduce dynamic characteristics observed in the baroreflex neural arc (20, 22).

Finally, we measured renal SNA as a proxy of systemic sympathetic activity. SNAs to different organs may vary a lot. Although static and dynamic regulations of the baroreflex neural arc are similar among renal, cardiac, and muscle SNAs (15, 16, 18), whether this holds true during muscle stretch remains to be verified. Also, subsystems of the peripheral arc transfer function such as those relating cardiac output and peripheral vascular resistance remain to be identified.

Conclusions. In conclusion, baroreflex open-loop transfer function analysis demonstrated that the activation of mechanosensitive afferents from skeletal muscles augmented the dynamic SNA response in the neural arc. This augmentation of the dynamic SNA response with maintained derivative characteristics of the neural arc may accelerate closed-loop AP regulation via the baroreflex.

APPENDIX

To simulate the closed-loop AP response to stepwise pressure perturbation (Fig. 6), we used the derivative-sigmoidal cascade model. The cascade model consists of a linear derivative filter followed by a nonlinear sigmoidal component (20, 22).

We modeled the sigmoidal nonlinearity in the baroreflex neural arc interacting with the muscle mechanoreflex by the following four-parameter logistic function with threshold according to a previous study (59):

$$y = \max\left\{\frac{P_1}{1+\exp[P_2(x-P_3)]} + P_4,\ \mathrm{Th}\right\} \qquad (A1)$$

where x and y are input (in mmHg) and output (in au) values. P_1 denotes the response range (in au), P_2 is the coefficient of gain, P_3 is the midpoint of the input range (in mmHg), P_4 is the minimum output value of the symmetric sigmoid curve (in au), and Th is a threshold value for the output (in au). The function $\max\{a,b\}$ gives the greater or equal value between a and b. We set $P_1 = 135$ au, $P_2 = 0.13$, $P_3 = 110$ mmHg, $P_4 = -40$ au, and Th = 0 au. Under muscle stretch conditions, the value of P_4 was changed to 5 au. These settings were determined based on the static interaction

between the baroreflex and muscle mechanoreflex obtained from previous studies (58, 59).

The sigmoidal nonlinearity in the peripheral arc was modelled by a four-parameter logistic function as follows:

$$z = \frac{Q_1}{1 + \exp[Q_2(y - Q_3)]} + Q_4 \qquad (A2)$$

where y and z are input (in au) and output (in mmHg) values. Q_1 denotes the response range (in mmHg), Q_2 is the coefficient of gain, Q_3 is the midpoint of the input range (in au), and Q_4 is the minimum output value (in mmHg). We set Q_1 = 120 mmHg, Q_2 = −0.05, Q_3 = 70 au, and Q_4 = 30 mmHg under both conditions, according to a previous study (58).

The neural arc (H_N) and peripheral arc (H_P) linear transfer functions under control and muscle stretch conditions were obtained from Fig. 2. Because absolute values of the steady-state gains in the neural and peripheral arcs were determined by a sigmoid curve (*Eqs. A1* and *A2*), the steady-state gains of H_N and H_P under both conditions were normalized to unity.

The input amplitude of the stepwise pressure perturbation was −40 mmHg. To mimic pulsatile pressure, we imposed a sinusoidal input on the output from the peripheral arc. The frequency and zero to peak amplitude of the sinusoidal input were 4 Hz and 15 mmHg, respectively (Fig. 6*A*). The closed-loop AP response was simulated up to 30 s (Fig. 6*B*).

GRANTS

This work was supported by Ministry of Health, Labour and Welfare of Japan Health and Labour Sciences Research Grant for Research on Advanced Medical Technology, Health and Labour Sciences Research Grant for Research on Medical Devices for Analyzing, Supporting and Substituting the Function of Human Body, and Health and Labour Sciences Research Grants H18-Iryo-Ippan-023 and H18-Nano-Ippan-003; the Industrial Technology Research Grant Program of the New Energy and Industrial Technology Development Organization of Japan; and Ministry of Education, Culture, Sports, Science and Technology Grant-In-Aid for Scientific Research 18591992.

REFERENCES

1. **Charkoudian N, Martin EA, Dinenno FA, Eisenach JH, Dietz NM, Joyner MJ.** Influence of increased central venous pressure on baroreflex control of sympathetic activity in humans. *Am J Physiol Heart Circ Physiol* 287: H1658–H1662, 2004.
2. **Chen CY, Horowitz JM, Bonham AC.** A presynaptic mechanism contributes to depression of autonomic signal transmission in NTS. *Am J Physiol Heart Circ Physiol* 277: H1350–H1360, 1999.
3. **Fadel PJ, Ogoh S, Watenpaugh DE, Wasmund W, Olivencia-Yurvati A, Smith ML, Raven PB.** Carotid baroreflex regulation of sympathetic nerve activity during dynamic exercise in humans. *Am J Physiol Heart Circ Physiol* 280: H1383–H1390, 2001.
4. **Gallagher KM, Fadel PJ, Smith SA, Norton KH, Querry RG, Olivencia-Yurvati A, Raven PB.** Increases in intramuscular pressure raise arterial blood pressure during dynamic exercise. *J Appl Physiol* 91: 2351–2358, 2001.
5. **Gallagher KM, Fadel PJ, Stromstad M, Ide K, Smith SA, Querry RG, Raven PB, Secher NH.** Effects of exercise pressor reflex activation on carotid baroreflex function during exercise in humans. *J Physiol* 533: 871–880, 2001.
6. **Gallagher KM, Fadel PJ, Stromstad M, Ide K, Smith SA, Querry RG, Raven PB, Secher NH.** Effects of partial neuromuscular blockade on carotid baroreflex function during exercise in humans. *J Physiol* 533: 861–870, 2001.
7. **Hayes SG, Kaufman MP.** Gadolinium attenuates exercise pressor reflex in cats. *Am J Physiol Heart Circ Physiol* 280: H2153–H2161, 2001.
8. **Hayes SG, Kindig AE, Kaufman MP.** Comparison between the effect of static contraction and tendon stretch on the discharge of group III and IV muscle afferents. *J Appl Physiol* 99: 1891–1896, 2005.
9. **Ichinose M, Saito M, Fujii N, Ogawa T, Hayashi K, Kondo N, Nishiyasu T.** Modulation of the control of muscle sympathetic nerve activity during incremental leg cycling. *J Physiol* 586: 2753–2766, 2008.
10. **Ichinose M, Saito M, Kondo N, Nishiyasu T.** Time-dependent modulation of arterial baroreflex control of muscle sympathetic nerve activity during isometric exercise in humans. *Am J Physiol Heart Circ Physiol* 290: H1419–H1426, 2006.
11. **Ichinose M, Saito M, Wada H, Kitano A, Kondo N, Nishiyasu T.** Modulation of arterial baroreflex control of muscle sympathetic nerve activity by muscle metaboreflex in humans. *Am J Physiol Heart Circ Physiol* 286: H701–H707, 2004.
12. **Ichinose M, Saito M, Wada H, Kitano A, Kondo N, Nishiyasu T.** Modulation of arterial baroreflex dynamic response during muscle metaboreflex activation in humans. *J Physiol* 544: 939–948, 2002.
13. **Iellamo F, Legramante JM, Raimondi G, Peruzzi G.** Baroreflex control of sinus node during dynamic exercise in humans: effects of central command and muscle reflexes. *Am J Physiol Heart Circ Physiol* 272: H1157–H1164, 1997.
14. **Ikeda Y, Kawada T, Sugimachi M, Kawaguchi O, Shishido T, Sato T, Miyano H, Matsuura W, Alexander J Jr, Sunagawa K.** Neural arc of baroreflex optimizes dynamic pressure regulation in achieving both stability and quickness. *Am J Physiol Heart Circ Physiol* 271: H882–H890, 1996.
15. **Kamiya A, Kawada T, Yamamoto K, Michikami D, Ariumi H, Miyamoto T, Shimizu S, Uemura K, Aiba T, Sunagawa K, Sugimachi M.** Dynamic and static baroreflex control of muscle sympathetic nerve activity (SNA) parallels that of renal and cardiac SNA during physiological change in pressure. *Am J Physiol Heart Circ Physiol* 289: H2641–H2648, 2005.
16. **Kamiya A, Kawada T, Yamamoto K, Michikami D, Ariumi H, Miyamoto T, Uemura K, Sugimachi M, Sunagawa K.** Muscle sympathetic nerve activity averaged over 1 minute parallels renal and cardiac sympathetic nerve activity in response to a forced baroreceptor pressure change. *Circulation* 112: 384–386, 2005.
17. **Kamiya A, Michikami D, Fu Q, Niimi Y, Iwase S, Mano T, Suzumura A.** Static handgrip exercise modifies arterial baroreflex control of vascular sympathetic outflow in humans. *Am J Physiol Regul Integr Comp Physiol* 281: R1134–R1139, 2001.
18. **Kawada T, Shishido T, Inagaki M, Tatewaki T, Zheng C, Yanagiya Y, Sugimachi M, Sunagawa K.** Differential dynamic baroreflex regulation of cardiac and renal sympathetic nerve activities. *Am J Physiol Heart Circ Physiol* 280: H1581–H1590, 2001.
19. **Kawada T, Shishido T, Inagaki M, Zheng C, Yanagiya Y, Uemura K, Sugimachi M, Sunagawa K.** Estimation of baroreflex gain using a baroreflex equilibrium diagram. *Jpn J Physiol* 52: 21–29, 2002.
20. **Kawada T, Uemura K, Kashihara K, Kamiya A, Sugimachi M, Sunagawa K.** A derivative-sigmoidal model reproduces operating point-dependent baroreflex neural arc transfer characteristics. *Am J Physiol Heart Circ Physiol* 286: H2272–H2279, 2004.
21. **Kawada T, Yamamoto K, Kamiya A, Ariumi H, Michikami D, Shishido T, Sunagawa K, Sugimachi M.** Dynamic characteristics of carotid sinus pressure-nerve activity transduction in rabbits. *Jpn J Physiol* 55: 157–163, 2005.
22. **Kawada T, Yanagiya Y, Uemura K, Miyamoto T, Zheng C, Li M, Sugimachi M, Sunagawa K.** Input-size dependence of the baroreflex neural arc transfer characteristics. *Am J Physiol Heart Circ Physiol* 284: H404–H415, 2003.
23. **Kawada T, Zheng C, Yanagiya Y, Uemura K, Miyamoto T, Inagaki M, Shishido T, Sugimachi M, Sunagawa K.** High-cut characteristics of the baroreflex neural arc preserve baroreflex gain against pulsatile pressure. *Am J Physiol Heart Circ Physiol* 282: H1149–H1156, 2002.
24. **Keller DM, Fadel PJ, Ogoh S, Brothers RM, Hawkins M, Olivencia-Yurvati A, Raven PB.** Carotid baroreflex control of leg vasculature in exercising and non-exercising skeletal muscle in humans. *J Physiol* 561: 283–293, 2004.
25. **Leshnower BG, Potts JT, Garry MG, Mitchell JH.** Reflex cardiovascular responses evoked by selective activation of skeletal muscle ergoreceptors. *J Appl Physiol* 90: 308–316, 2001.
26. **Liu Z, Chen CY, Bonham AC.** Frequency limits on aortic baroreceptor input to nucleus tractus solitarii. *Am J Physiol Heart Circ Physiol* 278: H577–H585, 2000.
27. **Marmarelis PZ, Marmarelis VZ.** The white noise method in system identification. In: *Analysis of Physiological Systems*. New York: Plenum, 1978, p. 131–221.
28. **Matsukawa K, Nakamoto T, Inomoto A.** Gadolinium does not blunt the cardiovascular responses at the onset of voluntary static exercise in cats: a predominant role of central command. *Am J Physiol Heart Circ Physiol* 292: H121–H129, 2007.

29. **McIlveen SA, Hayes SG, Kaufman MP.** Both central command and exercise pressor reflex reset carotid sinus baroreflex. *Am J Physiol Heart Circ Physiol* 280: H1454–H1463, 2001.
30. **Melcher A, Donald DE.** Maintained ability of carotid baroreflex to regulate arterial pressure during exercise. *Am J Physiol Heart Circ Physiol* 241: H838–H849, 1981.
31. **Mense S, Stahnke M.** Responses in muscle afferent fibres of slow conduction velocity to contractions and ischaemia in the cat. *J Physiol* 342: 383–397, 1983.
32. **Miki K, Yoshimoto M, Tanimizu M.** Acute shifts of baroreflex control of renal sympathetic nerve activity induced by treadmill exercise in rats. *J Physiol* 548: 313–322, 2003.
33. **Miles R.** Frequency dependence of synaptic transmission in nucleus of the solitary tract in vitro. *J Neurophysiol* 55: 1076–1090, 1986.
34. **Mohrman DE, Heller LJ.** Regulation of arterial pressure. In: *Cardiovascular Physiology* (4th ed.). New York: McGraw-Hill, 1997, p. 158–230.
35. **Norton KH, Boushel R, Strange S, Saltin B, Raven PB.** Resetting of the carotid arterial baroreflex during dynamic exercise in humans. *J Appl Physiol* 87: 332–338, 1999.
36. **Ogoh S, Fisher JP, Dawson EA, White MJ, Secher NH, Raven PB.** Autonomic nervous system influence on arterial baroreflex control of heart rate during exercise in humans. *J Physiol* 566: 599–611, 2005.
37. **Ogoh S, Fisher JP, Fadel PJ, Raven PB.** Increases in central blood volume modulate carotid baroreflex resetting during dynamic exercise in humans. *J Physiol* 581: 405–418, 2007.
38. **Ogoh S, Fisher JP, Raven PB, Fadel PJ.** Arterial baroreflex control of muscle sympathetic nerve activity in the transition from rest to steady-state dynamic exercise in humans. *Am J Physiol Heart Circ Physiol* 293: H2202–H2209, 2007.
39. **Ogoh S, Wasmund WL, Keller DM, AOY, Gallagher KM, Mitchell JH, Raven PB.** Role of central command in carotid baroreflex resetting in humans during static exercise. *J Physiol* 543: 349–364, 2002.
40. **Papelier Y, Escourrou P, Gauthier JP, Rowell LB.** Carotid baroreflex control of blood pressure and heart rate in men during dynamic exercise. *J Appl Physiol* 77: 502–506, 1994.
41. **Papelier Y, Escourrou P, Helloco F, Rowell LB.** Muscle chemoreflex alters carotid sinus baroreflex response in humans. *J Appl Physiol* 82: 577–583, 1997.
42. **Potts JT, Hand GA, Li J, Mitchell JH.** Central interaction between carotid baroreceptors and skeletal muscle receptors inhibits sympathoexcitation. *J Appl Physiol* 84: 1158–1165, 1998.
43. **Potts JT, Li J.** Interaction between carotid baroreflex and exercise pressor reflex depends on baroreceptor afferent input. *Am J Physiol Heart Circ Physiol* 274: H1841–H1847, 1998.
44. **Potts JT, Mitchell JH.** Rapid resetting of carotid baroreceptor reflex by afferent input from skeletal muscle receptors. *Am J Physiol Heart Circ Physiol* 275: H2000–H2008, 1998.
45. **Potts JT, Shi XR, Raven PB.** Carotid baroreflex responsiveness during dynamic exercise in humans. *Am J Physiol Heart Circ Physiol* 265: H1928–H1938, 1993.
46. **Querry RG, Smith SA, Stromstad M, Ide K, Raven PB, Secher NH.** Neural blockade during exercise augments central command's contribution to carotid baroreflex resetting. *Am J Physiol Heart Circ Physiol* 280: H1635–H1644, 2001.
47. **Rowell LB, O'Leary DS.** Reflex control of the circulation during exercise: chemoreflexes and mechanoreflexes. *J Appl Physiol* 69: 407–418, 1990.
48. **Sato T, Kawada T, Inagaki M, Shishido T, Takaki H, Sugimachi M, Sunagawa K.** New analytic framework for understanding sympathetic baroreflex control of arterial pressure. *Am J Physiol Heart Circ Physiol* 276: H2251–H2261, 1999.
49. **Smith SA, Querry RG, Fadel PJ, Gallagher KM, Stromstad M, Ide K, Raven PB, Secher NH.** Partial blockade of skeletal muscle somatosensory afferents attenuates baroreflex resetting during exercise in humans. *J Physiol* 551: 1013–1021, 2003.
50. **Stebbins CL, Brown B, Levin D, Longhurst JC.** Reflex effect of skeletal muscle mechanoreceptor stimulation on the cardiovascular system. *J Appl Physiol* 65: 1539–1547, 1988.
51. **Sugimachi M, Imaizumi T, Sunagawa K, Hirooka Y, Todaka K, Takeshita A, Nakamura M.** A new method to identify dynamic transduction properties of aortic baroreceptors. *Am J Physiol Heart Circ Physiol* 258: H887–H895, 1990.
52. **Suzuki S, Ando S, Imaizumi T, Takeshita A.** Effects of anesthesia on sympathetic nerve rhythm: power spectral analysis. *J Auton Nerv Syst* 43: 51–58, 1993.
53. **Terui N, Masuda N, Saeki Y, Kumada M.** Activity of barosensitive neurons in the caudal ventrolateral medulla that send axonal projections to the rostral ventrolateral medulla in rabbits. *Neurosci Lett* 118: 211–214, 1990.
54. **Vatner SF, Braunwald E.** Cardiovascular control mechanisms in the conscious state. *N Engl J Med* 293: 970–976, 1975.
55. **Vatner SF, Franklin D, Braunwald E.** Effects of anesthesia and sleep on circulatory response to carotid sinus nerve stimulation. *Am J Physiol* 220: 1249–1255, 1971.
56. **Vatner SF, Franklin D, Van Citters RL, Braunwald E.** Effects of carotid sinus nerve stimulation on blood-flow distribution in conscious dogs at rest and during exercise. *Circ Res* 27: 495–503, 1970.
57. **Wray DW, Fadel PJ, Keller DM, Ogoh S, Sander M, Raven PB, Smith ML.** Dynamic carotid baroreflex control of the peripheral circulation during exercise in humans. *J Physiol* 559: 675–684, 2004.
58. **Yamamoto K, Kawada T, Kamiya A, Takaki H, Miyamoto T, Sugimachi M, Sunagawa K.** Muscle mechanoreflex induces the pressor response by resetting the arterial baroreflex neural arc. *Am J Physiol Heart Circ Physiol* 286: H1382–H1388, 2004.
59. **Yamamoto K, Kawada T, Kamiya A, Takaki H, Sugimachi M, Sunagawa K.** Static interaction between muscle mechanoreflex and arterial baroreflex in determining efferent sympathetic nerve activity. *Am J Physiol Heart Circ Physiol* 289: H1604–H1609, 2005.

REGULAR PAPER

J. Physiol. Sci. Vol. 58, No. 3; Jun. 2008; pp. 189–198
Online May 13, 2008; **doi:10.2170/physiolsci.RP004308**

Upright Tilt Resets Dynamic Transfer Function of Baroreflex Neural Arc to Minify the Pressure Disturbance in Total Baroreflex Control

Atsunori KAMIYA[1], Toru KAWADA[1], Kenta YAMAMOTO[2], Masaki MIZUNO[1], Shuji SHIMIZU[1], and Masaru SUGIMACHI[1]

[1]Department of Cardiovascular Dynamics, National Cardiovascular Centre Research Institute, Osaka, Japan; and [2]Consolidated Research Institute for Advanced Science and Medical Care, Waseda University, Tokyo ,162-0041 Japan

Reprinted from
The Journal of Physiological Sciences
Volume 58, Number 3, pp. 189–198, 2008
http://jps.physiology.jp/ doi:10.2170/physiolsci.RP004308

Published by The Physiological Society of Japan

Received on Mar 18, 2008; accepted on May 9, 2008; released online on May 13, 2008; doi:10.2170/physiolsci.RP004308
Correspondence should be addressed to: Atsunori Kamiya, Department of Cardiovascular Dynamics, National Cardiovascular Centre Research Institute, Osaka, 565-8565 Japan. Tel: +81-6-6833-5012, Fax: +81-6-6835-5403, E-mail: kamiya@ri.ncvc.go.jp

REGULAR PAPER

J. Physiol. Sci. Vol. 58, No. 3; Jun. 2008; pp. 189–198
Online May 13, 2008; doi:10.2170/physiolsci.RP004308

Upright Tilt Resets Dynamic Transfer Function of Baroreflex Neural Arc to Minify the Pressure Disturbance in Total Baroreflex Control

Atsunori KAMIYA[1], Toru KAWADA[1], Kenta YAMAMOTO[2], Masaki MIZUNO[1], Shuji SHIMIZU[1], and Masaru SUGIMACHI[1]

[1]Department of Cardiovascular Dynamics, National Cardiovascular Centre Research Institute, Osaka, Japan; and [2]Consolidated Research Institute for Advanced Science and Medical Care, Waseda University, Tokyo ,162-0041 Japan

Abstract: Maintenance of arterial pressure (AP) under orthostatic stress against gravitational fluid shift and pressure disturbance is of great importance. One of the mechanisms is that upright tilt resets steady-state baroreflex control to a higher sympathetic nerve activity (SNA). However, the dynamic feedback characteristics of the baroreflex system, a hallmark of fast-acting neural control, remain to be elucidated. In the present study, we tested the hypothesis that upright tilt resets the dynamic transfer function of the baroreflex neural arc to minify the pressure disturbance in total baroreflex control. Renal SNA and AP were recorded in ten anesthetized, vagotomized and aortic-denervated rabbits. Under baroreflex open-loop condition, isolated intracarotid sinus pressure (CSP) was changed according to a binary white noise sequence at operating pressure ± 20 mmHg, while the animal was placed supine and at 60° upright tilt. Regardless of the postures, the baroreflex neural (CSP to SNA) and peripheral (SNA to AP) arcs showed dynamic high-pass and low-pass characteristics, respectively. Upright tilt increased the transfer gain of the neural arc (resetting), decreased that of the peripheral arc, and consequently maintained the transfer characteristics of total baroreflex feedback system. A simulation study suggests that postural resetting of the neural arc would significantly increase the transfer gain of the total arc in upright position, and that in closed-loop baroreflex the resetting increases the stability of AP against pressure disturbance under orthostatic stress. In conclusion, upright tilt resets the dynamic transfer function of the baroreflex neural arc to minify the pressure disturbance in total baroreflex control.

Key words: baroreflex, blood pressure, sympathetic nervous system.

Since human beings are often under orthostatic stress, the maintenance of arterial pressure (AP) under orthostatic stress against gravitational fluid shift is of great importance. During standing, a gravitational fluid shift directed toward the lower part of the body would cause severe postural hypotension if not counteracted by compensatory mechanisms [1]. Arterial baroreflex has been considered to be the major compensatory mechanism [1–3], since denervation of baroreceptor afferents causes profound postural hypotension [4].

The baroreflex system consists of two subsystems: the neural arc that represents the input-output relationship between baroreceptor pressure and sympathetic nerve activity (SNA), and the peripheral arc that represents the relationship between SNA and systemic AP. Recently, we investigated the steady-state functional structure of these systems under orthostatic stress [5], and reported that upright tilt shifted the baroreflex peripheral arc to a lower AP for a given SNA. However, upright tilt reset the baroreflex neural arc to a higher steady state SNA. The resetting compensated for the blunted responsiveness of the peripheral arc and contributed to prevent postural hypotension [5].

In addition to the steady state characteristics [6, 7], the dynamic characteristics are other hallmark of the baroreflex system. It is because the system is a fast-acting neural control that quickly negative-feedback controls and stabilises AP against pressure disturbance in contrast to the slow-acting hormonal and humoral systems [8]. Earlier studies reported that the dynamic characteristics in supine position have a high-pass (fast) neural arc that may compensate for the low-pass (slow) peripheral arc to achieve rapid and stable AP regulation [8]. The importance of the dynamic characteristics in AP control increases under orthostatic stress that can cause postural hypotension. However, little is known about the dynamic characteristics of the baroreflex system in upright posture.

Because the gravitational body fluid shift decreases the effective circulatory blood volume [1, 9], we speculated that upright tilt may attenuate the dynamic transfer function from SNA to AP in the baroreflex peripheral arc.

Received on Mar 18, 2008; accepted on May 9, 2008; released online on May 13, 2008; doi:10.2170/physiolsci.RP004308
Correspondence should be addressed to: Atsunori Kamiya, Department of Cardiovascular Dynamics, National Cardiovascular Centre Research Institute, Osaka, 565-8565 Japan. Tel: +81-6-6833-5012, Fax: +81-6-6835-5403, E-mail: kamiya@ri.ncvc.go.jp

Moreover, if the upright tilt resets the dynamic characteristics of the neural arc in addition to resetting the steady state SNA reported previously [5], it would compensate for a blunted pressor response of the baroreflex peripheral arc and contribute to maintain the stability and quickness of the total baroreflex system. Accordingly, we hypothesized that upright tilt resets dynamic transfer function of baroreflex neural arc to minify the pressure disturbance in total baroreflex control.

In the present study, we identified the transfer functions of two baroreflex subsystems (the neural and peripheral arcs) separately in 60° upright posture, while opening the baroreflex negative feedback loop by vascular isolation of carotid sinus regions [8]. In addition, by connecting the subsystem transfer functions in series and closing them, we investigated the dynamic transfer characteristics and the stability against pressure disturbance of total baroreflex arc system in upright posture.

MATERIAL AND METHODS

Animals were cared for in strict accordance with the Guiding Principles for the Care and Use of Animals in the Field of Physiological Science approved by the Physiological Society of Japan. Ten Japanese white rabbits weighing 2.4–3.3 kg were initially anesthetized by intravenous injection (2 ml/kg) of a mixture of urethane (250 mg/ml) and α-chloralose (40 mg/ml). Anesthesia was maintained by continuously infusing the anaesthetics at a rate of 0.33 ml/kg/h using a syringe pump (CFV-3200, Nihon Kohden, Tokyo). The rabbits were mechanically ventilated with oxygen-enriched room air. Bilateral carotid sinuses were isolated vascularly from systemic circulation by ligating the internal and external carotid arteries and other small branches originating from the carotid sinus regions. The isolated carotid sinuses were filled with warmed physiological saline pre-equilibrated with atmospheric air, through catheters inserted via the common carotid arteries. Intra-carotid sinus pressure (CSP) was controlled by a servo-controlled piston pump (model ET-126A, Labworks; Costa Mesa, CA). Bilateral vagal and aortic depressor nerves were sectioned in the middle of the neck region to eliminate reflexes from the cardiopulmonary region and the aortic arch. Systemic AP was measured using a high-fidelity pressure transducer (Millar Instruments; Houston, TX) inserted retrograde from the right common carotid artery below the isolated carotid sinus region. Body temperature was maintained at around 38°C with a heating pad.

The left renal sympathetic nerve was exposed retroperitoneally. A pair of stainless steel wire electrodes (Bioflex wire AS633, Cooner Wire) was attached to the nerve to record renal SNA. The nerve fibers peripheral to electrodes were ligated securely and crushed to eliminate afferent signals. The nerve and electrodes were covered with a mixture of silicone gel (Silicon Low Viscosity, KWIK-SIL, World Precision Instrument, Inc., FL) to insulate and immobilize the electrodes. The preamplified SNA signal was band-pass filtered at 150–1,000 Hz. The nerve signal was full-wave rectified and low-pass filtered with a cutoff frequency of 30 Hz to quantify the nerve activity.

Protocols. Both protocols 1 and 2 were performed on each of eight animals. After the surgical preparation, the animal was maintained supine (0°) on a tilt bed. To stabilize the posture, the head was fixed full-frontal to the bed by strings, and the body and legs were rigged up in a clothes-like bag. Before performing protocols 1 and 2, we confirmed that the nerve activity measured in supine position was SNA. CSP was decreased stepwise from 100 mmHg to 40 mmHg in decrements of 20 mmHg, and then increased stepwise to 100 mmHg in increments of 20 mmHg. Each pressure step was maintained for 60 s. In all animals, a decrease in CSP increased SNA, whereas an increase in CSP decreased SNA (Fig. 1), indicating that the nerve activity recorded was SNA.

Protocol 1: The animal was placed supine. CSP was firstly matched with systemic AP to obtain the operating AP under the baroreflex closed-loop condition. After at least 5 minutes of stabilization, the SNA and AP were recorded for 10 min to obtain closed-loop baseline values. The data were stored on the hard disk of a dedicated laboratory computer system for analysis at a sampling rate of 200 Hz using a 12-bit analog-to-digital converter. The averaged AP over 10 min was defined as the operating AP in

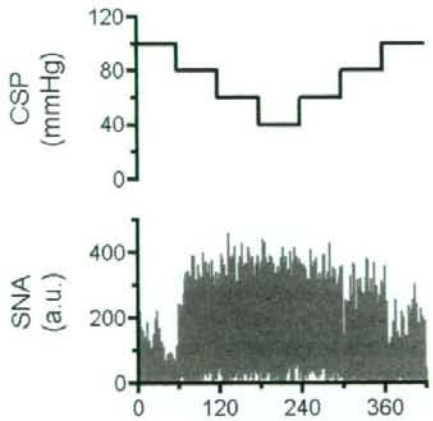

Fig. 1. Representative data of one rabbit in supine position, showing time series of carotid sinus pressure (CSP) and sympathetic nerve activity (SNA). CSP was decreased stepwise from 100 mmHg to 40 mmHg in decrements of 20 mmHg, and then increased stepwise to 100 mmHg in increments of 20 mmHg. Each pressure step was maintained for 60 s. A decrease in CSP increased SNA, whereas an increase in CSP decreased SNA, indicating that the nerve activity recorded was SNA. a.u., arbitrary unit.

supine position. Then, after at least 5 min of stabilization, CSP was randomly changed by 20 mmHg above or below the operating AP every 500 ms according to a binary white noise sequence for which the input power spectrum of CSP was reasonably flat up to 1 Hz [10]. The variables were recorded for a 10-min period and stored.

Protocol 2: CSP was firstly matched with systemic AP via a servo-controlled piston pump to obtain the actual operating pressure under baroreflex closed-loop conditions in supine and 60° upright postures. The animal was maintained supine for 10 min, and then tilted upright to 60° within 10 s by inclining the tilt bed to 60° and dropping the lower regions of the rabbit with the fulcrum set at the level of the carotid sinus. The 60° upright posture was maintained for 10 min for stabilization. Since the clothes-like bag stabilized the posture of the animal, there was no additional mechanical movement that reduced the quality of measurements. The position of the head remained almost fixed during the tilt to minimize vestibular stimulation. Thereafter, the average AP over the next 10 min was defined as the operating AP in upright tilt position. Then, after at least 5 min of stabilization, CSP was randomly changed according to a white noise sequence for 10 min as in protocol 1.

Data analysis. SNA signals were normalized by the following steps. First, the post-mortem noise level was assigned 0 arbitrary unit (a.u.). Second, SNA signals during the 10-min closed-loop baseline recording in protocol 1 (supine position) were averaged over 1 min, and assigned 100 a.u. Finally, the other SNA signals in all protocols were normalized to these values.

In both protocols 1 and 2, the transfer functions (gain and phase) and coherence function were calculated from CSP input to SNA in the baroreflex neural arc and from SNA input to AP in the baroreflex peripheral arc. The signals of CSP, SNA and AP were resampled at 10 Hz and segmented into 10 sets of 50% overlapping bins of 2^{10} data point each. The segment length was 102.4 s, which yielded the lowest frequency bound of 0.01 (0.0097) Hz. We subtracted a linear trend and applied a Hanning window for each segment. We then performed fast Fourier transform to obtain frequency spectra of the variables. We ensemble averaged the input power [$Sxx(f)$], output power [$Syy(f)$], and cross power between them [$Syx(f)$] over the 10 segments. Thereafter, we calculated the transfer function [$H(f)$] from input to output signals as follows,

$$H(f) = \frac{Syx(f)}{Sxx(f)}$$

To quantify the linear dependence between input to output signals in the frequency domain, we calculated the magnitude-squared coherence function [$Coh(f)$] as follows:

$$Coh(f) = \frac{|Syx(f)|^2}{Sxx(f)Syy(f)}$$

The coherence value ranges from zero to unity. Unity coherence indicates a perfect linear dependence between input and output signals, whereas zero coherence indicates total independence of these two signals.

Statistic analysis. All data are presented as means ± SD. Effects of upright tilt on baroreflex parameters were evaluated by repeated-measures analysis of variance. When the main effect was found to be significant, post hoc multiple comparisons were done using the Scheff's F-test to compare baroreflex controls between the supine and upright postures [11]. Differences were considered significant when $P < 0.05$.

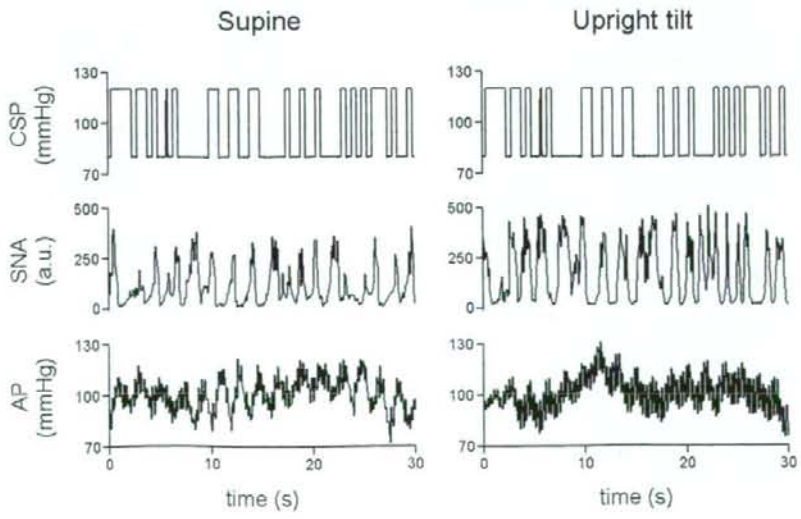

Fig. 2. Representative data of one rabbit in supine (left panels) and 60° upright tilt (right panels) positions, showing time series of carotid sinus pressure (CSP), sympathetic nerve activity (SNA) and systemic arterial pressure (AP) during CSP perturbation. CSP was changed according to a binary white noise signal with a switching interval of 500 ms. a.u., arbitrary unit.

RESULTS

Figure 2 shows the typical time series of CSP, SNA and AP derived in supine and 60° upright tilt positions in individual animal. CSP was perturbed according to a binary white noise sequence at 500-ms intervals. In both positions, SNA increased and decreased roughly in response to the decrease and increase in CSP, respectively. However, the SNA responses appeared higher in the upright tilt than in the supine position. Data from all animals (n = 8) showed that the upright tilt increased the averaged SNA (175 ± 21 a.u.) during CSP perturbation compared with the supine position (96 ± 13 a.u.). Averaged AP during CSP perturbation was similar in supine (96 ± 13 mmHg) and in upright positions (103 ± 15 mmHg).

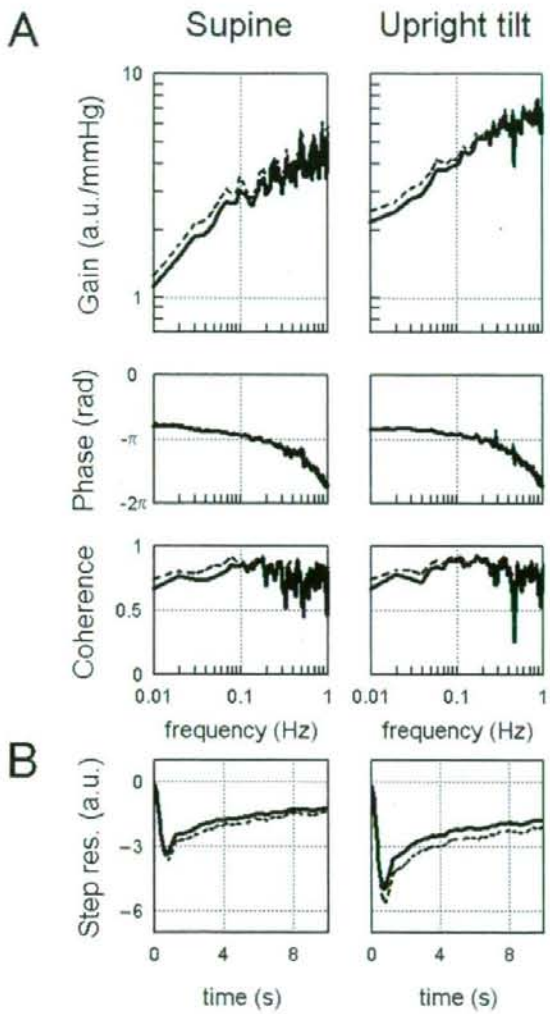

Fig. 3. A: The transfer function of the baroreflex neural arc from CSP to SNA averaged from all animals (n = 8) in supine (left panels) and 60° upright tilt (right panels) positions. The gain plots (top), phase plots (middle), and coherence function (bottom) are shown. Upright tilt increases the gain. **B**: Step responses (Step res.) derived from the transfer function corresponding to the transfer function shown in A. Upright tilt enhances the initial and steady-state responses. Solid line represents the mean values, and dashed line represents mean + SD in A and mean − SD in B. a.u., arbitrary unit.

The baroreflex neural arc

Figure 3A shows the transfer function of baroreflex neural arc from CSP to SNA averaged from all animals. In both supine and upright tilt positions, the transfer gain increased as the frequency of CSP perturbation increased for the frequency range of 0.01 to 1 Hz. This shows dynamic high-pass characteristics, indicating that more rapid change of CSP results in greater response of SNA. Note that upright tilt increased the transfer gain for the whole frequency range observed (Table 1). In addition, upright tilt decreased the slope of gain increase. In both positions, the phase approached slightly above $-\pi$ radians at the lowest frequency reflecting negative feedback characters, and lagged as the frequency of CSP perturbation increased. The coherence was over 0.7 for the frequency range of 0.01 to 0.2 Hz. Upright tilt did not affect the phase or coherence. Figure 3B shows the step response of SNA corresponding to the transfer function shown in Fig. 3A. In both positions, the SNA response consisted of an initial decrease followed by partial recovery and then a steady state. Of note, upright tilt enhanced the initial decrease by 50%, and also decreased the steady-state SNA.

Table 1. Transfer function of baroreflex neural arc (from CSP to SNA) in supine and upright tilt positions.

	Supine	Upright tilt
Gain (a.u./mmHg)		
0.01 Hz	1.11 ± 0.13	2.14 ± 0.41*
0.1 Hz	2.75 ± 0.43	4.63 ± 0.52*
0.3 Hz	3.69 ± 0.30	5.08 ± 0.42*
Phase (rad)		
0.01 Hz	−2.51 ± 0.15	−2.66 ± 0.09
0.1 Hz	−2.96 ± 0.08	−2.93 ± 0.06
0.3 Hz	−3.58 ± 0.14	−3.53 ± 0.12
Coherence		
0.01 Hz	0.67 ± 0.08	0.67 ± 0.07
0.1 Hz	0.84 ± 0.04	0.89 ± 0.02
0.3 Hz	0.77 ± 0.06	0.82 ± 0.03
Slope (dB/decade)		
0.01 Hz to 0.3 Hz	7.0 ± 0.4	5.1 ± 0.5*
Step response (a.u.)		
Initial response	−3.41 ± 0.21	−4.99 ± 0.62*
Steady-state level	−1.26 ± 0.18	−1.80 ± 0.32*

Values are mean ± SD (n =10). *P < 0.05; supine position vs. upright tilt.

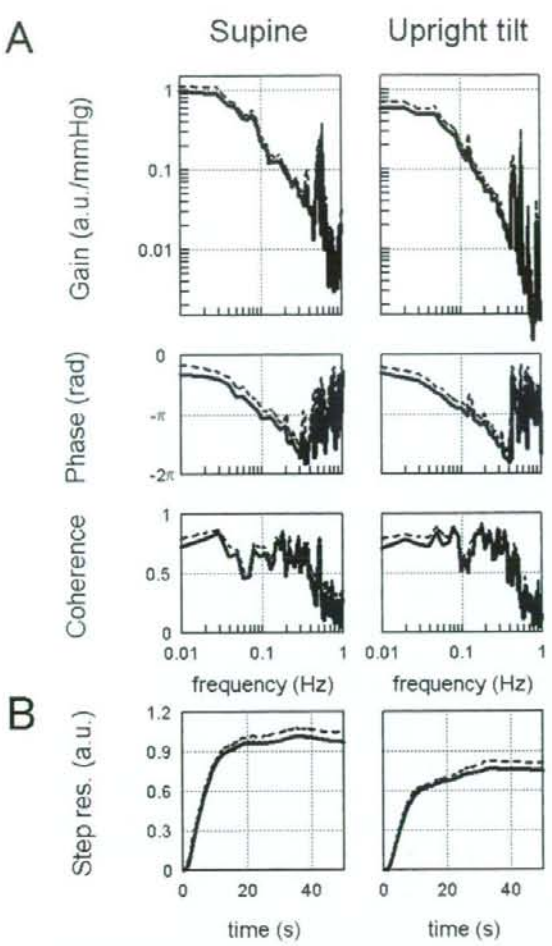

Fig. 4. A: The transfer function of the baroreflex peripheral arc from SNA to AP averaged from all animals (n = 8) in supine (left panels) and 60° upright tilt (right panels) positions. The gain plots (top), phase plots (middle), and coherence function (bottom) are shown. Upright tilt decreases the gain below the frequency of 0.1 Hz. **B**: Step responses (Step res.) derived from the transfer function corresponding to the transfer function shown in A. Upright tilt attenuates the response. Solid and dashed lines represent the mean and mean + SD values, respectively. a.u., arbitrary unit.

Table 2. Transfer function of baroreflex peripheral arc (from SNA to AP) in supine and upright tilt positions.

	Supine	Upright tilt
Gain (mmHg/au)		
0.01 Hz	0.97 ± 0.09	0.63 ± 0.06*
0.1 Hz	0.23 ± 0.03	0.15 ± 0.03*
0.3 Hz	0.04 ± 0.006	0.03 ± 0.003
Phase (rad)		
0.01 Hz	−0.79 ± 0.16	−0.69 ± 0.07
0.1 Hz	−2.83 ± 0.14	−2.58 ± 0.15
0.3 Hz	−4.74 ± 0.18	−4.63 ± 0.08
Coherence		
0.01 Hz	0.72 ± 0.07	0.71 ± 0.03
0.1 Hz	0.64 ± 0.08	0.62 ± 0.04
0.3 Hz	0.61 ± 0.08	0.68 ± 0.02
Step response (mmHg)		
Steady-state level	−0.97 ± 0.06	−0.75 ± 0.06*

Values are mean ± SD (n =10). *P < 0.05; supine position vs. upright tilt.

The baroreflex peripheral arc

Figure 4A shows the transfer function of the baroreflex peripheral arc from SNA to AP averaged from all animals. In both supine and upright tilt positions, the transfer gain decreased as the input frequency increased for the frequency range of 0.01 to 1 Hz, indicating low-pass characteristics. Upright tilt decreased the transfer gain between 0.01 and 0.1 Hz (Table 2). In both positions, the phase approached zero radian at the lowest frequency reflecting an increase in SNA with increased AP, and lagged as the input frequency increased. The coherence was over 0.5 for the frequency range of 0.01 to 1 Hz. Upright tilt did not affect the phase or coherence. Figure 4B shows the step response of AP corresponding to the transfer function shown in Fig. 4A. In both positions, the AP response increased gradually to reach a steady state. Upright tilt decreased the steady-state AP.

The total baroreflex arc

Figure 5A shows the transfer function of the total baroreflex arc from CSP to AP averaged from all animals. In both supine and upright tilt positions, the transfer gain decreased as the input frequency increased for the frequency range from 0.01 to 1 Hz, indicating low-pass characteristics. Upright tilt did not affect the transfer gain (Table 3). In both positions, the phase approached $-\pi$ radians at the lowest frequency reflecting negative feedback attained by the total baroreflex loop, and lagged as the input frequency increased. The coherence was over 0.5 for the frequency range from 0.01 to 0.2 Hz. Upright tilt did not affect the phase or coherence. Figure 5B shows the step response of AP corresponding to the transfer function shown in Fig. 5A. In both positions, the AP response increased gradually to reach a steady state. Upright tilt did not affect the step response.

The right column of Table 3 shows a simulation of the total arc transfer function in the absence of resetting in the neural arc. The simulation was based on the neural arc transfer function in supine position and the peripheral arc transfer function in upright tilt position. Without the resetting, the upright tilt would decrease the transfer function gain and would attenuate the step response of AP at steady state, compared with the values in supine position and those in upright tilt position with resetting.